[American Journal of Science, Vol. 322, April, 2022, P. 561–592, DOI 10.2475/04.2022.02]

FROM GONDWANA RIFTING TO ALPINE OROGENY: DETRITAL ZIRCON GEOCHRONOLOGIC AND PROVENANCE SIGNALS FROM THE KOPET DAGH BASIN (NE IRAN)

ALI MOHAMMADI*,†, JONAS B. RUH**, MARCEL GUILLONG**, OSCAR LAURENT**.***, and LOTFOLLAH AGHAJARI§

ABSTRACT. The Kopet Dagh mountains in NE Iran exhibit a 7-km-thick continuous sedimentary sequence recording detritus from exposed surrounding terranes from the last 175 Ma. This work presents a multi-disciplinary geochronologic and provenance analysis in an attempt to identify and date major geologic events along the northern segment of the Tethys and reconstruct the regional tectonic history from Gondwana-related rifting until the Alpine orogeny. Sandstone framework, heavy mineral analysis, U-Pb dating of detrital zircons, and Hf-isotope ratio measurements on dated zircons from Triassic to Paleocene sandstones indicate three main tectonic events that include Early Silurian intracontinental rifting (opening of Paleo-Tethys), Early Carboniferous rifting of a back-arc basin (Aghdarband Complex), and Late Triassic collisional to post-collisional magmatism (Paleo-Tethys collision). Mineralogical and age peak considerations indicate that detritus was supplied from the south into the extensional Kopet Dagh Basin during Middle Jurassic, while Cretaceous to Paleocene sandstones show signs of increasing recycling.

Key words: Kopet Dagh Basin, Gondwana, Paleo-Tethys, Neo-Tethys, Rifting, Collision, Detrital zircon, Hf isotopes, Provenance anlysis

INTRODUCTION

The long-standing tectonic history between Gondwana and Eurasia includes several phases of rifting and collision, recorded by magmatic and metamorphic episodes in various domains of related orogenic belts; from the Alps in the west to the Himalayas in the east (for example Stöcklin, 1974; Şengör, 1990a; 1990b; Stampfli, 2000). The timing of the main tectonic episodes including rifting, subduction initiation, and collision are crucial for the reconstruction of plate tectonics (for example Stampfli and Borel, 2002). Geochronology and geochemistry of magmatic and metamorphic rocks are widely applied in geodynamic studies to constrain the timing and other characteristics of such tectonic events (for example Barbarin, 1999; Brown, 2014). However, the occurrence and surface exposure of such igneous and metamorphic terranes may be limited in some tectono-sedimentary domains because of complete erosion or coverage by younger sediments. In addition, the application of different dating methods on igneous and metamorphic rocks provides a wide range of ages, which makes the exact timing of tectonic events difficult. In fact, timing constraints for tectonic events based only on magmatic or metamorphic rocks may not be comprehensive. A more accurate detection of large-scale tectonic events can be found in clastic sedimentary successions, where the source of detritus rapidly responds to any plate tectonic reorganization (Fedo and others, 2003; Cawood and others, 2012). Therefore, provenance analysis, zircon geochronology, and zircon isotopic

* Eurasia Institute of Earth Sciences, Istanbul Technical University, Maslak, Istanbul, Turkey
** Department of Earth Sciences, ETH Zürich, Sonneggstrasse 5, 8092 Zürich, Switzerland
*** CNRS, Géosciences Environnement Toulouse, Observatoire Midi-Pyrénées, 14 avenue Edouard Belin F-31400 Toulouse, France
§ Exploration Directorate, National Iranian Oil Company, Sheikh Baha'i Square, Seoul Street, Tehran, Iran
† Corresponding author: mohammadiali@itu.edu.tr

composition on detrital sandstones may help to improve the precision when constraining the timing of tectonic events (for example, Weltje and von Eynatten, 2004; Cawood and others, 2012).

Several episodes of continental rifting and collision took place between Gondwana and Eurasia since the Palaeozoic until the Cenozoic that ultimately climaxed in the Alpine-Himalayan orogeny (for example Stöcklin, 1974; Şengör and others, 1984; Stampfli, 2000; Stampfli and Borel, 2002). Separation of several continental slivers and microcontinental blocks from Gondwana occurred in two phases, coeval with the opening of two ocean basins, the Paleo-Tethys and Neo-Tethys oceans (for example Stöcklin, 1974; Şengör and others, 1984; Alavi, 1996; Stampfli, 2000; Cawood and others, 2021). The opening of the Iranian segment of the Paleo-Tethys between the Iranian continent (Gondwana) and the Turan platform (Eurasia) was suggested to have occurred in the Early Palaeozoic (Ordovician-Silurian) based on ages of oceanic basalts from eastern Alborz (Boulin, 1988; Stampfli, 2000). The subsequent northwards subduction of the Paleo-Tethys beneath Eurasia initiated during the Late Devonian and continued until the Late Triassic as shown from dating of the Darrehanjir–Mashhad ophiolites (for example, Stampfli, 2000; Wilmsen and others, 2009; Moghadam and others, 2015a). The opening of a new ocean (Neo-Tethys Ocean) between the Arabian plate and the Central Iran block during the Permian went hand in hand with the northward movement of the Central Iran block, resulting in the closure of the Paleo-Tethys Ocean in Late Triassic, and the consequent collision of the Iranian plate with the Turan block; the Cimmerian orogeny (for example Berberian and King, 1981; Muttoni and others, 2009; Zanchetta and others, 2013; Delavari and others, 2016). This Cimmerian orogeny prevented further shortening along the northern segment of the Tethys and triggered the onset of subduction of the southern Neo-Tethys Ocean (for example, Zanchetta and others, 2013).

The northward subduction of the Neo-Tethys Ocean beneath the Central Iran block was accompanied by the opening of the Greater Caucasus–South Caspian–Kopet Dagh basins during the Middle Mesozoic, potentially in form of a larger back-arc basin (Alavi and others, 1997; Brunet and Cloetingh, 2003; Zanchi and others, 2006). The Neo-Tethys Ocean finally closed during the collision of the Arabian plate and Central Iran block in late Early Oligocene, which resulted in the Alpine orogeny (Cai and others, 2021). This collision related to the closure of the Neo-Tethys resulted in tectonic inversion of previously extensional domains (Greater Caucasus, South Caspian, and Kopet Dagh basins) along the Paleo-Tethys suture (for example, Robert and others, 2014; Ruh and Vergés, 2018).

The Kopet Dagh Basin contains a stratigraphic record covering the last ~175 Ma (Middle Jurassic to Neogene sedimentary succession; Afshar-Harb, 1982a; Moussavi-Harami and Brenner, 1990). Detailed provenance analysis of this shallowing-upward (deep marine–marine–deltaic–continental) sequence allows i) to reconstruct the Mesozoic-Tertiary sedimentary evolution of the Kopet Dagh Basin, ii) to clarify the general tectonic setting associated with the Turan and Iran plates, and finally iii) to constrain the timing of rifting and collision events related to the opening and closure of the Paleo-Tethys and Neo-Tethys oceans.

In this study, we present combined results from sandstone modal framework, heavy mineral assemblage analysis, detrital zircon U-Pb age, and *in situ* Hf isotope composition of Triassic (pre-rift basement), and Middle Jurassic to Paleocene detrital sediments from the Kopet Dagh. Results are interpreted to identify and characterize the respective source rocks in terms of ages and genesis. Based on these data, we determine the provenance of sedimentary detritus and reconstruct the variety of rift-related, continental arc, and post-collisional tectonic settings from Gondwana-related rifting (opening of Paleo-Tethys) to Alpine orogeny (closure of Neo-Tethys).

GOLOGY OF THE KOPET DAGH

Tectonic Setting

The Kopet Dagh mountains in NE Iran strike over 700 km along the Iran–Turkmenistan border and form the northern limit of the Alpine-Himalayan orogeny (Golonka, 2004: Robert and others, 2014; fig. 1). The Main Kopet Dagh Fault (MKF) and the East Alborz and Binalud mountains mark the northern and the southern boundary of the Kopet Dagh Basin, respectively (fig. 1). Tectonically, the Kopet Dagh Basin was interpreted to have formed as an extensional back-arc basin to the Neo-Tethys subduction system farther to the south (Mangino and Priestley, 1998; Brunet and Cloetingh, 2003). The onset of extension is marked by a major nonconformity, and rapid sediment facies and thickness variations in the Middle Jurassic (165 Ma to 170 Ma) deep-marine turbiditic sediments (Thomas and others, 1999; Robert and others, 2014; Kavoosi and others, 2009). In contrast to the Caspian Sea Basin in the west, there is no evidence for formation of oceanic crust beneath the Kopet Dagh Basin (Brunet and others, 2003). After this rifting event, the basin experienced a

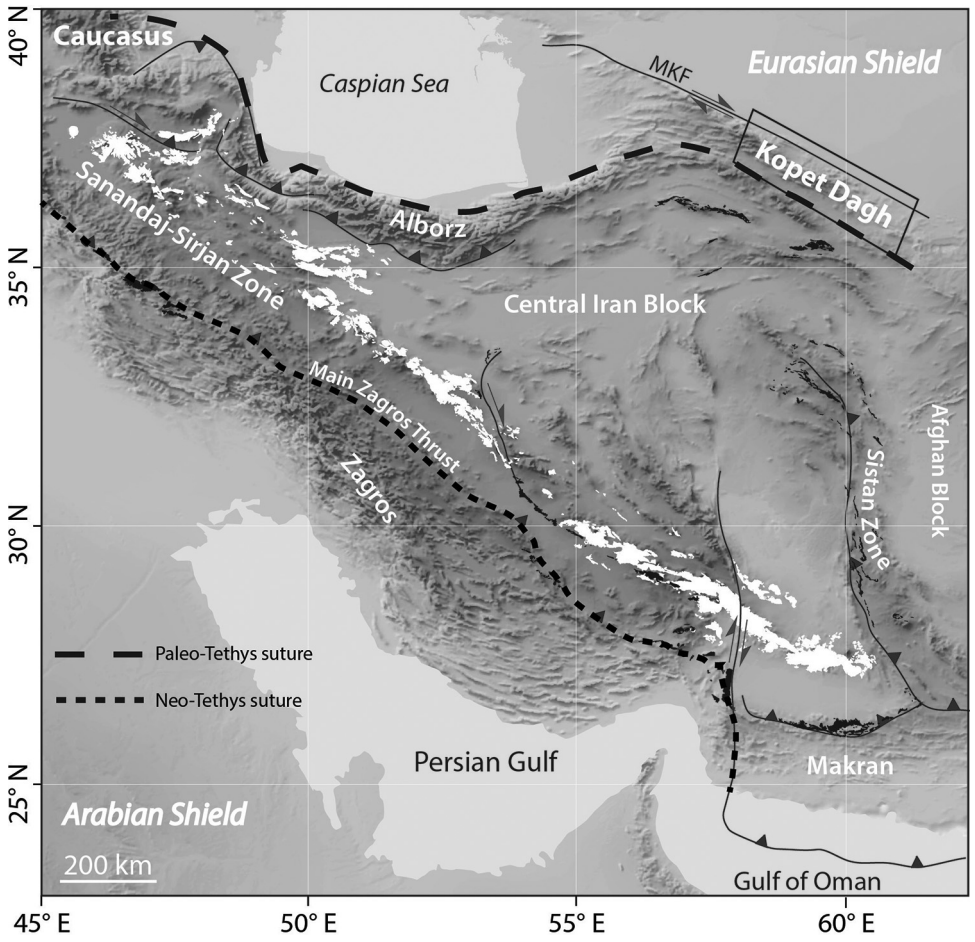

Fig. 1. Simplified tectonic setting of Iran including Urumieh Dokhtar Magmatic Arc (white) and the Tethys ophiolite complexes (black). Framed: eastern Kopet Dagh Basin. Background: shaded relief map ETOPO1 (http://www.ngdc.noaa.gov/mgg/global/relief/ETOPO1).

phase of tectonic quiescence for at least 130 Ma until Oligocene-Miocene, when the extensional basins along the Paleo-Tethys suture experienced tectonic inversion (for example, Lyberis and Manby, 1999; Hollingsworth and others, 2010) as a consequence of the Arabian-Eurasian collision (Zagros orogeny) that resulted in newly arranged relative plate motions (McQuarrie and others, 2003). Inversion of the Kopet Dagh mountains is synchronous with the onset of deposition of continental sedimentary facies (Robert and others, 2014) and resulted in widespread folding and faulting of the Jurassic to Tertiary stratigraphy with an estimated N-S shortening of ~75 km (Lyberis and Manby, 1999; Allen and others, 2003). The compressional phase continued for about 15 Ma, with an increased component of dextral strike-slip movement since ~10 Ma (Hollingsworth and others, 2006).

Stratigraphy

The study area is located in the eastern part of the Kopet Dagh Basin covered by the Darreh Gaz, Mashhad, Sarakhs, Torbat-e-Heydarieh, and Torbat-e-Jam 1:250,000 geological maps published by the Geological Survey of Iran (figs. 1, 2; Afshar-Harb, 1982a, 1982b; Afshar and others, 1986; Vaezi Pour and others, 1992; Behrouzi and others, 1993). An up to seven-kilometers-thick terrigenous and carbonate sedimentary

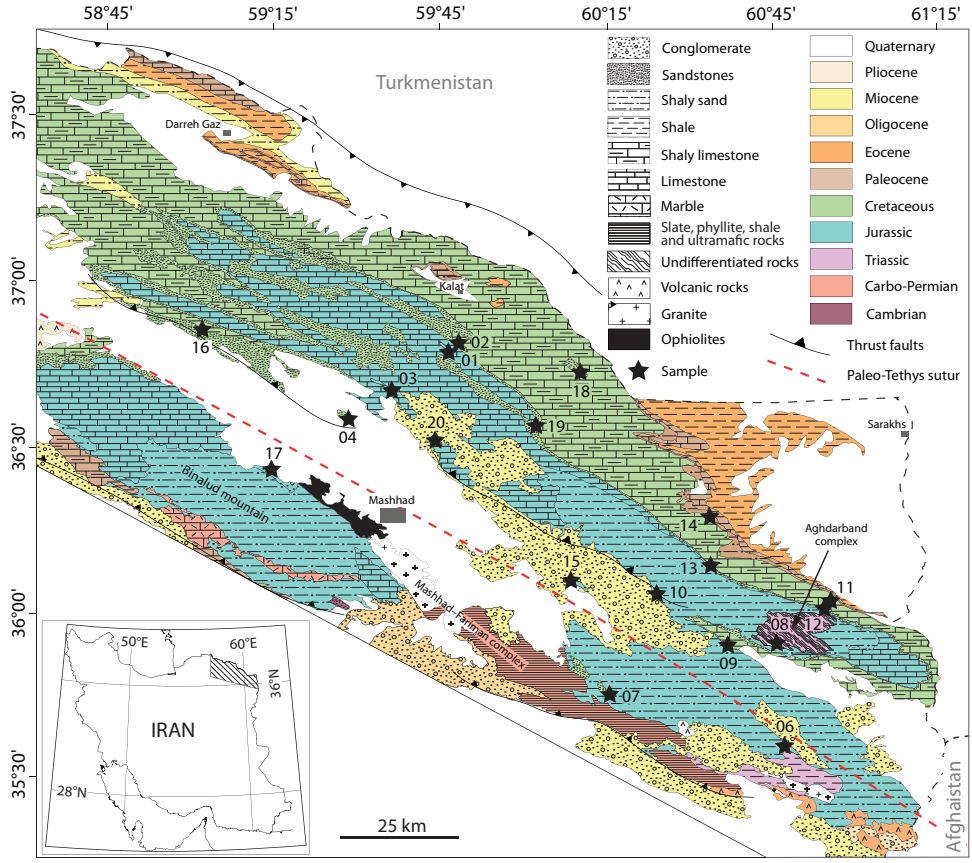

Fig. 2. Simplified geologic map of the East Kopet Dagh Basin and samples location. Stratigraphic ages correspond to the 1:250,000 geological maps of Sarakhs (Afshar-Harb, 1982a), Darreh Gaz (Afshar-Harb, 1982b), Mashhad (Afshar-Harb and others, 1986), and Torbat-e-Jam (Behrouzi and others, 1993).

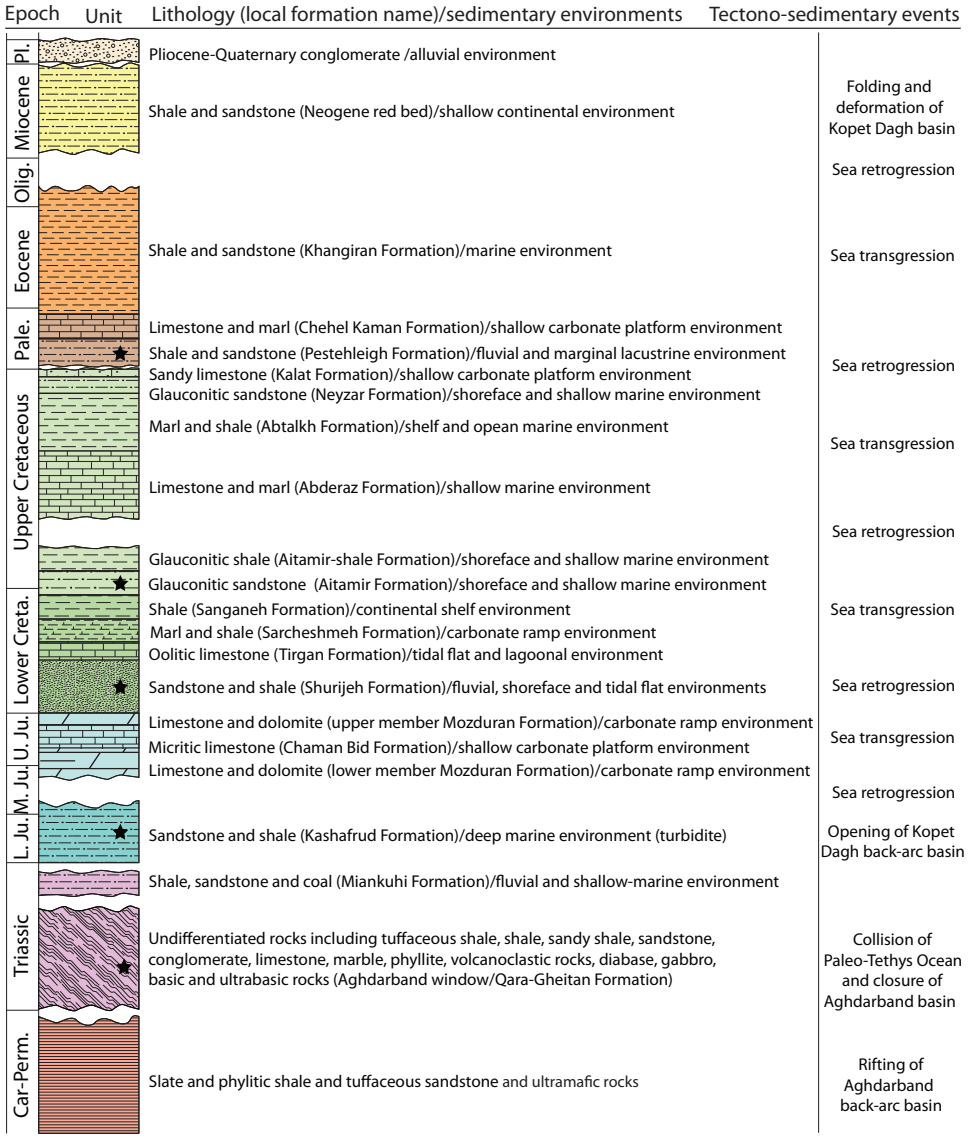

Fig. 3. Composite stratigraphic description of the East Kopet Dagh Basin with local formation names, sampled formations, comments on lithology and sedimentary environment, and the major tectono-stratigraphic events. Stratigraphic ages correspond to the 1:250,000 geological maps of Sarakhs (Afshar-Harb, 1982a), Darreh Gaz (Afshar-Harb, 1982b), Mashhad (Afshar-Harb and others, 1986), and Torbat-e-Jam (Behrouzi and others, 1993). Black stars: sampled sedimentary sequences.

succession was deposited into the Kopet Dagh Basin between Middle Jurassic to Neogene (figs. 2, 3; Moussavi-Harami and Brenner, 1990). The Middle Jurassic (Late Bajocian to Bathonian) interval of deep marine turbiditic conglomerate, thin- and thick-bedded sandstones, siltstone, and mudstone (Kashafrud Formation) are the oldest sediments deposited into the Kopet Dagh Basin (for example, Poursoltani, and others, 2007; Poursoltani and Gibling, 2011). Middle Jurassic sedimentary rocks rest unconformably on Triassic mafic intrusions and volcanogenic sedimentary rocks and exhibit variations in thickness across major extensional basement faults, indicating a

syn-rifting depositional environment (Thomas and others, 1999; Robert and others, 2014). Thickness of the turbiditic sediments vary between 280 m and over 2000 m in the East Kopet Dagh Basin (fig. 3). The Middle Jurassic turbiditic succession is unconformably overlain by Upper Jurassic (Callovian-Kimmeridgian) thick (>1200 m) marine carbonates and shallow marine, coastal plain silisiclastic sediments (Mozduran Formation; Lasemi, 1995; Kavoosi and others, 2009; fig. 3). Thick fluvial siliciclastic sediments of Early Cretaceous age (Surijeh Formation) record epicontinental sea retogradation in the eastern part of the Kopet Dagh Basin (fig. 3; Moussavi-Harami and Brenner, 1990). Contemporaneous deposition of marine carbonate indicates the presence of a marine environment in the western Kopet Dagh Basin. Further transgression established a marine depositional environment throughout the entire Kopet Dagh Basin until Late Cretaceous time (Turonian). This transgressive system is characterized by intervals of oolitic limestone (Tirgan Formation), marl and shale (Sarcheshmeh Formation), shale (Sanganeh Formation), and glauconitic-carbonatic sandstone and shale (Aitamir Formation; fig. 3). This wide range of lithologies indicates sea level fluctuation and deposition in tidal flat, lagoonal, carbonate ramp, shoreface, and continetal shelf environments. A short-lived retogression during the Late Cretaceous (Turonian) is responsible for an unconformity between the shallow marine glauconitic shale (Aitamir Formation) and shallow marine marl and limestones (Abderaz Formation; fig. 3). Between the Turonian and the Paleocene, the East Kopet Dagh Basin experienced other transgressive episodes characterized by deposition of shallow marine marl and limestones (Abderaz Formation), shelf and open marine marl and shale (Abtalkh Formation), shallow marine and shoreface glauconitic sandstone (Neyzar Formation), and shallow carbonate platform sandy limestones (Kalat Formation; fig. 3). Basin-scale sea retrogression and surface exposure of strata is recorded by erosional surfaces within the uppermost part of Upper Cretaceous sandy limestones (Kalat Formation; Mahboubi and others, 2006). In the Early Paleocene, reddish fluvial and lacustrine mudstones and sandstones (Pestehleigh Formation) were unconformably deposited onto uppermost Cretaceous marine sediments. During the Late Paleocene, the Kopet Dagh Basin gradualy changed from a shallow continental sedimentary environment to a shallow carbonate paltform with marl and limestones (Chehel Kaman Formation). The basin subsidence continued until Eocene-Early Oligocene time, when marine shale and sandstones (Khangiran Formation) conformably overlayed Upper Paleocene sediments. Repeated minor transgressions and regressions followed into the Miocene, until the basin was tectonically inverted duing the Alpine orogeny, accompanied by deposition of continental conglomerate, sandstone, and shale (Neogene red beds; fig. 3).

METHODS

Nineteen sandstone samples including one sandstone sample of a lens within Triassic polymictic conglomerate, and eighteen well-cemented medium-grained Jurassic to Paleocene turbiditic, fluvial-deltaic, and continental sandstone samples were investigated (with prefix KD-01–20 in the ETH collection). Studied sandstones represent five different litho-stratigraphic formations (Qara-Gheitan, Kashafrud, Shurijeh, Aitamir, and Pestehleigh formations) of the Kopet Dagh Basin (figs 1, 2, 3, and table S1). We combined sandstone framework composition and heavy mineral analysis, detrital zircon U-Pb geochronology, and *in situ* Hf-isotopic composition to reconstruct the lithological composition of the source-rocks and the tectonic evolution of the source area.

Sandstone Petrography

Sandstones modal framework analysis was performed with the Gazzi-Dickinson method (Ingersoll and others, 1984), whereby grains or crystals larger than >63 μm

within lithic fragments falling under the cross-hair were counted as monomineralic grains. Only aphanitic fragments were included in the lithic-fragment portion and other mono-mineralic polycrystalline grains were excluded. At least 300 grains were counted in each thin section (Zuffa, 1985), previously stained for carbonates and feldspars (Dickson, 1966; Norman, 1974). Results were converted to percentages for compositional comparison (Weltje and von Eynatten, 2004; table S2). Four standard complementary triangular diagrams were used to display the data (QFL, QmPK, QFL, and LvLmLs; Dickinson, 1985; Garzanti, 2016).

Heavy Mineral Separation

Approximately 2 to 3 kg of fresh rock were collected at each sample site for heavy mineral analysis. To obtain heavy mineral fractions, sandstones were crushed with the SelFrag apparatus batch equipment using high voltage (130–150 kV) pulse power technology, which liberates morphologically intact minerals. From the <2 mm sieved fraction, carbonate was dissolved in warm (60–70°C), 10%-acetic acid. Heavy minerals were pulled out in separation funnels (Mange and Maurer, 1992) from 63 to 400 μm wet sieve fractions using bromoform (density 2.88 g/cm^3). The heavy mineral grains largely range between 63 μm and 150 μm. Only in one out of ten samples grains were >200 μm. The bulk heavy mineral fractions were mounted in piperine (Martens, 1932) between a glass slab and a cover. Identification and quantification were carried out under a petrographic microscope by applying the mid-point ribbon and fleet counting methods. At least 200 grains were counted per sample (Mange and Maurer, 1992; table S3).

Zircon Geochronology

Zircons were extracted from 2 to 3 kg of fresh sandstones crushed with the SelFrag apparatus. Standard Holman-Wilfley shaking tables and magnetic separation methods (Frantz magnetic separator) delivered mineral fractions enriched in zircons. Zircons of grain fraction 60 to 250 μm (non-magnetic) were handpicked under a binocular microscope. To avoid biases in the selection of coarse zircon grains during handpicking (Vermeesch and others 2017), we tried to pick zircons equally from different sizes and shapes, and not focusing on coarse grains. Selected grains were mounted in U- and Pb-free resin, polished to expose the internal parts of the minerals, and coated with carbon. Suitable zircon domains and inclusions were identified by cathodoluminescence (CL) and backscattered-electron (BSE) images obtained by split screen on a CamScan CS44 Scandunk Viermalning electron microscope (SEM; Tescan a.s., Brno) at ETH Zurich, and analyzed with laser ablation inductively coupled mass spectrometry (LA-ICP-MS) at ETH Zurich with an excimer laser (ArF 193 nm).

The laser ablation ICP-MS analyses were performed with a RESOlution (Australian Scientific Instruments/Applied Spectra) laser ablation system at ETH Zurich equipped with a dual-volume S-155 ablation cell (Laurin Technic, Australia), coupled to an Element XR (Thermo Scientific, Germany) sector-field ICP-MS. A laser repetition rate of 5 Hz, energy density of *ca.* 2.5 J/cm^2, and spot diameter of 30 μm were applied. The carrier gas consisted of high-purity He (*ca.* 0.7 L/min) and make-up Ar (*ca.* 1 L/min) from the ICP-MS. Data acquisition time per spot was about 1 minute (30 s gas blank + 30 s ablation). The data were processed with the Igor Pro Iolite v2.5 software (Hellstrom and others, 2008), using the VizualAge data reduction scheme (Petrus and Kamber, 2012). Laser-induced element fractionation (after Paton and others, 2010), instrumental mass discrimination, and drift through the analytical session were corrected by standard bracketing against zircon reference material "GJ-1" (using isotope ratios recommended by Horstwood and others, 2016). The quoted uncertainties for each individual analysis correspond to the internal error and propagated uncertainty based on the scatter of the

primary reference material (see Paton and others, 2010). The accuracy and reproducibility within each run of analyses were monitored by periodic measurements of zircon reference materials "Plešovice" (337 Ma; Sláma and others, 2008) and "91500" (1065 Ma; Wiedenbeck and others, 1995). More details about the analytical conditions, the data from unknowns and reference materials are provided in table S5. Concordia diagrams were obtained using ISOPLOT v.3.0 (Ludwig, 2003). A concordant age is given by the overlap of the error ellipse with the Concordia age curve. In this study, ages with discordance >5% are not included for further interpretation (table S4). The frequency U-Pb age distribution diagram or probability density plot described by Ludwig (2003) includes a histogram representing the number of individual zircon grains within a short age range, and the probability curve depicts the mean age peaks of the contained age populations in one sample.

Zircon Lu-Hf Isotopic Analyses

Lu–Hf analyses were obtained by laser ablation multi-collection inductively coupled plasma mass spectrometry (LA-MC-ICP-MS) at ETH Zurich, using a RESOlution (ASI/Applied Spectra) excimer (ArF) 193 nm laser ablation system attached to Nu Plasma II (Nu Instruments) multi-collector ICP-MS. A laser repetition rate of 5 Hz, a spot diameter of 50 μm, and a laser energy density of *ca.* 4 J/cm^2 was applied. Ablation was performed in a dual-volume, fast-washout S-155 ablation cell (Laurin Technic) fluxed with carrier gas consisting of *ca.* 0.37 L/min He and make-up gas consisting of *ca.* 0.92 L/min Ar. A typical run consisted of 40 s of background measurement followed by 40 s of sample ablation with an integration time of 0.5 s. The ICP-MS instrument was optimized for maximum sensitivity on ^{180}Hf, and optimal peak shape and coincidence for Yb, Lu, and Hf isotopes. The list of acquired masses and corresponding Faraday cups are provided in table S7.

The resulting intensities were processed offline with the Igor Pro Iolite v2.5 software, using an in-house data reduction scheme (Hellstrom and others, 2008). Background-subtracted intensities were used to calculate isotope ratios, which were corrected for instrumental mass bias by normalization to the natural abundance ratios ^{173}Yb/^{171}Yb (for both Yb and Lu isotope ratios) and ^{179}Hf/^{177}Hf (for Hf isotope ratios) of Chu and others (2002). The isobaric interferences of ^{176}Yb and ^{176}Lu on ^{176}Hf were subsequently corrected using the natural abundance ratios of ^{176}Yb/^{173}Yb = 0.79502 and ^{176}Lu/^{175}Lu = 0.02656. Accuracy and external reproducibility of the method were controlled by repeated analyses of reference zircon standards "GJ "(Morel and others, 2008), "Plešovice" (Sláma and others, 2008), "Mud Tank" and "Temora" (Woodhead and Hergt, 2005), and "QGNG" (Woodhead and others, 2004). The ^{176}Hf/^{177}Hf ratios obtained on all reference materials are within uncertainties identical to the recommended values. Calculations of initial ^{176}Hf/^{177}Hf ratios and ε-Hf were performed applying the ^{176}Lu decay constant of Scherer and others (2001) and ^{176}Hf/^{177}Hf and ^{176}Lu/^{177}Hf values for the chondritic uniform reservoir (CHUR) recommended by Bouvier and others (2008). The quoted uncertainties on initial Hf isotopic composition correspond to the analytical uncertainty and the average 2 S.D (table S6). Reproducibility of the initial Hf isotopic compositions of all measured zircon reference materials (table S7), were propagated by quadratic addition. More details about the analytical conditions, the data from unknowns, and reference materials are provided in table S7.

RESULTS

Sandstone Framework

The studied Triassic and Jurassic sandstones are mainly classified as feldspatho-litho-quartzose and litho-feldspatho-quartzose. Cretaceous sandstones are classified as

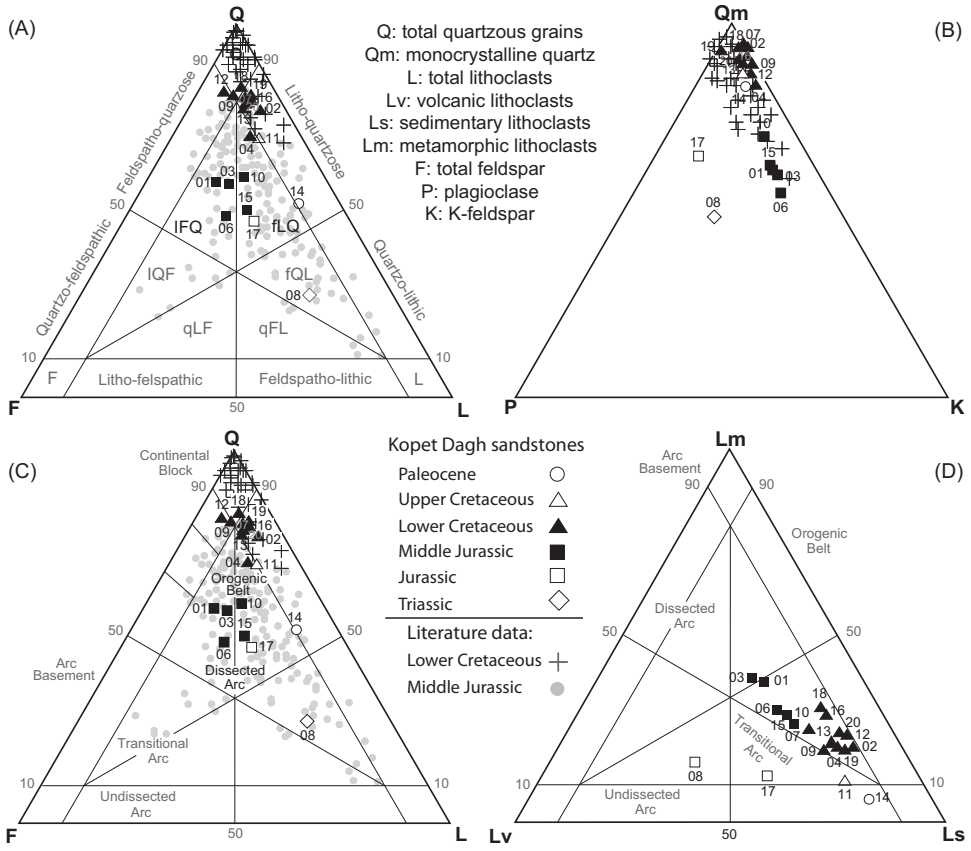

Fig. 4. Detrital composition of Kopet Dagh sandstones in ternary classification schemes and provenance discrimination diagrams. (A) Q-F-L sandstone classification diagram (Garzanti, 2016); (B) Qm-P-K diagram (after Dickinson and Suczek, 1979); (C) QFL diagram (Garzanti, 2016); (D) Lv-Lm-Ls diagram (Garzanti, 2016). Literature data of Middle Jurassic and Lower Cretaceous sandstones from Poursoltani and Gibling (2011) and Mortazavi and others, (2013).

quartz-rich feldspatho-quartzose and quartz-rich litho-quartzose. The Paleocene sandstone sample is a litho-quartzose (fig. 4A). Quartz grains of all samples are mostly monocrystalline (~50% in Triassic, 50–75% in Middle Jurassic, and >80% in Cretaceous and Paleocene sandstones; fig. 4A, B, C and table S2). K-feldspars are dominant among feldspar grains (~73% in the Jurassic, and ~80% in the Cretaceous and Paleocene sandstones; fig. 4B and table S2). From Jurassic to Cretaceous and Paleocene sandstones, the monocrystalline/polycrystalline quartz and K-feldspar/total feldspar ratios increase (fig. 4B). The Triassic sandstone is rich in volcanics (~55%), with less sedimentary and metamorphic lithics (~45%). Jurassic sandstones are composed of sedimentary (~60%), volcanic (~30%), and metamorphic (~10%) lithic grains. In Cretaceous and Paleocene sandstones, sedimentary and metamorphic lithics (together >95%) are dominant, while volcanic lithics are less common (<5%; fig. 4D and table S2). In both Jurassic and Cretaceous sandstones, sedimentary lithic grains mainly comprise siltstone, limestone, and dolomite, whereas metamorphic lithic grains generally consist of low-grade to medium-grade slate, phyllites, and schists. Volcanic lithic grains mainly represent andesite and volcanic glass. Dominantly volcanic lithics (fig. 4D) and pyroxene minerals (fig. 5) point toward a

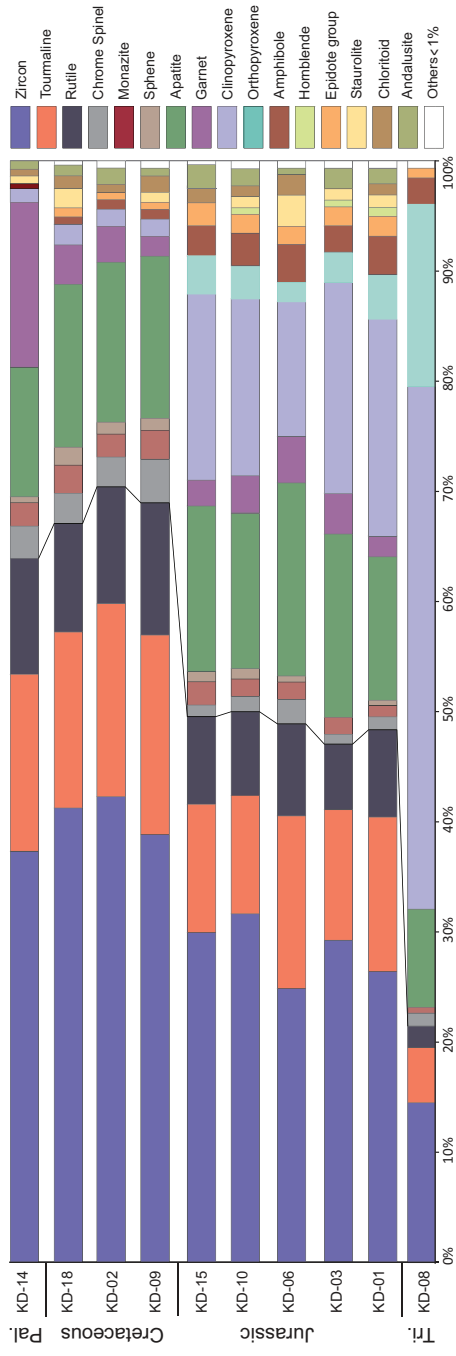

Fig. 5. Heavy mineral assemblages of the Kopet Dagh sandstones arranged by stratigraphic ages displaying the relative abundance of heavy mineral groups.

transitional arc as the source terrane of the Triassic sandstone, whereas Jurassic samples point to a dissected arc source, and Cretaceous and Paleocene sandstones show a recycling of older sediments (fig. 4C and D).

Heavy Mineral Study

Heavy mineral assemblages of sandstones from the Kopet Dagh are characterized as follows: (1) A group of more durable heavy minerals including zircon, tourmaline, and rutile (ZTR; Hubert 1962), sphene, monazite, and apatite. The amount of ZTR ranges from 22% of total dense fraction grain count in the Triassic sandstone and reaches up to 53% of total dense fraction grain count in Jurassic and up to 74.5% in Cretaceous sandstones (fig. 5). The percentage of apatite grains ranges between 9% in Triassic and 17.5% in Jurassic sandstones (fig. 5 and table S3). Around 10% of all apatite grains show signs of surface pitting. (2) Pyroxene and amphibole attributed to mafic magmatic, meta-igneous, and meta-sedimentary source rocks. The amount of pyroxene in Triassic sandstones reaches up to 64% of the total dense fraction grains, whereas Jurassic and Cretaceous sandstones contain 24% and 1.5% pyroxene (mainly clinopyroxene), respectively (fig. 5 and table S3). (3) A third group describes the epidote group, garnet, chloritoid, andalusite, and staurolite, that are common heavy minerals related to metamorphic rocks. The percentage of these minerals varies from 1% of total counted dense fraction grains in Triassic sandstones to 17% of total counted dense fraction grains in Paleocene sandstones (fig. 5 and table S3). (4) Fourth, Cr-spinel (up to 4% of total dense fraction grain count; fig. 5 and table S3) indicates dominant recycled older sediments and subordinary mafic-ultramafic rocks as sources of detritus.

Detrital Zircon U-Pb Ages

Laser ablation ICP-MS U-Pb dating on 2478 detrital zircon grains was conducted on one Lower Triassic low-grade meta-sandstone (Qara-Gheitan Formation), five Jurassic turbiditic sandstones (Kashafrud Formation), three Lower Cretaceous fluvial-deltaic sandstones (Shurijeh Formation), and one Paleocene continental sandstone (Pestehleigh Formation; figs. 2, 3, 6, 7, 8, 9, and tables S1 and S4).

Late Triassic (217 Ma) and Early Paleoproterozoic (2374 Ma) zircons are the youngest and oldest zircons of 232 analysed detrital zircons from the Lower Triassic sandstone (fig. 7; sample KD-08). This sandstone reveals a single probability peak at 337 Ma (Early Carboniferous). Five Jurassic sandstones show zircon age distributions between 154 Ma (Late Jurassic) and 2966 Ma (Mesoarchean) based on a total of 1191 dated grains (fig. 7; samples KD-01, KD-03, KD-06, KD-10, KD-15). Detrital zircons of the Jurassic sandstones display peaks at 232 Ma (early Late Triassic), 343 Ma (Early Carboniferous), 434 Ma (Early Silurian), 643 Ma (Middle Neoproterozoic), and 1833 Ma (Late Paleoproterozoic; fig. 7). A total of 865 zircons from three Lower Cretaceous sandstones revealed ages between Early Cretaceous (116 Ma) to Mesoarchean (2861 Ma) (fig. 8; samples KD-02, KD-09, KD-18). The Lower Cretaceous sandstones show a similar zircon age distribution as the Jurassic sandstones, with an additional zircon probability peak at 132 Ma (Early Cretaceous; fig. 8). The Paleocene sandstone shows ages ranging between 119 Ma (Early Cretaceous) and 2781 Ma (Neoarchean) from 190 dated zircon grains (fig. 8; sample KD-14). The probability peaks of Paleocene sandstone zircon ages are similar to the ones of Cretaceous sandstones (fig. 8). The combined zircon ages call attention to Late Paleoproterozoic, Middle Neoproterozoic, Early Silurian, Early Carboniferous, Late Triassic, and Early Cretaceous protoliths in the potential source areas (figs. 9 and 10).

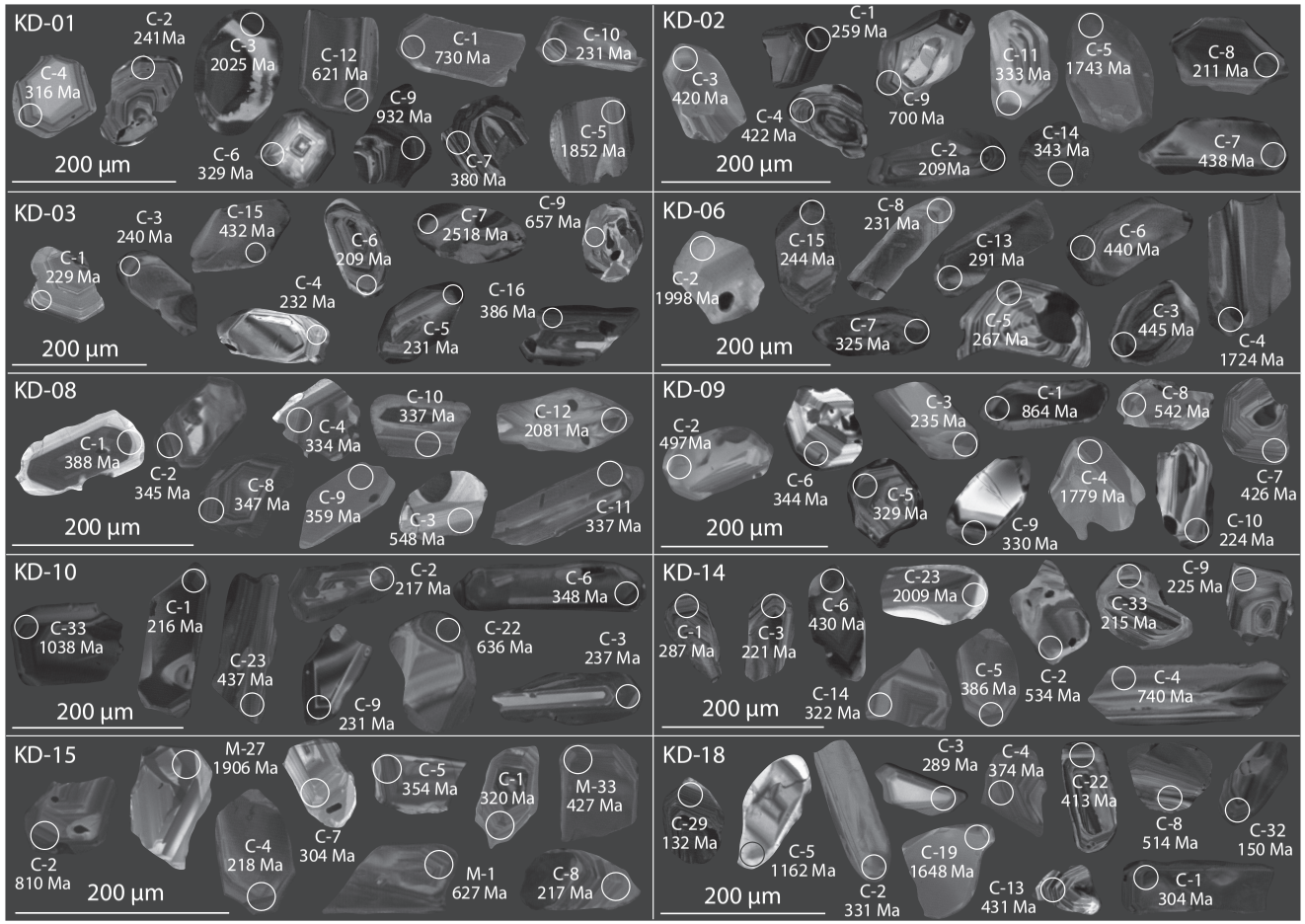

Fig. 6. Representative cathodoluminescence images of dated detrital zircons of the Kopet Dagh sandstones. White circles show laser spot positions for U-Pb age analyses.

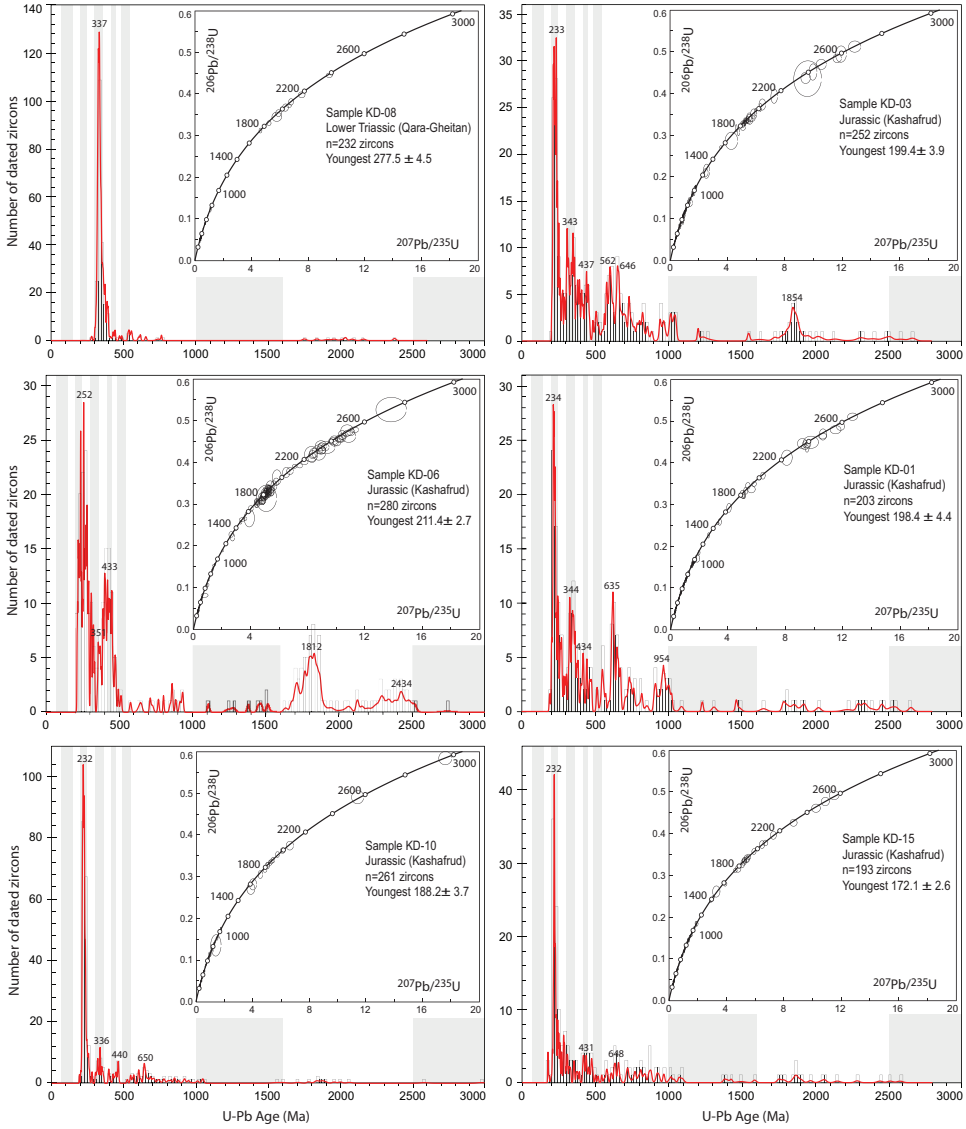

Fig. 7. Detrital zircon $^{206}Pb/^{238}U$ age probability density diagrams with corresponding Concordia plots for the Lower Triassic and Jurassic samples KD-01, KD-03, KD-06, KD-08, KD-10, and KD-15. Ages with discordance greater than 5% are excluded. Time scale after Gradstein and others (2012).

Hf Isotopic Composition

Hafnium isotopic composition analysis was conducted on 151 concordantly dated zircon grains with internal growth structures that were large and thick enough to be examined with laser beams. The overall Hf isotopic compositions (epsilon hafnium values: ε-$Hf_{(t)}$) of Triassic to Paleocene sandstones range from -23 to +15 (fig. 11). Late Paleoproterozoic zircon grains demonstrate evolved ε-$Hf_{(t)}$ values from -13 to +1. Early Silurian zircons show a mixed positive and negative pattern of ε-$Hf_{(t)}$ from -2 to +7 (fig. 11). Early Carboniferous zircons show positive ε-$Hf_{(t)}$ values of -1 to +12 with four grains between -17 and -4 (fig. 11). Similar to Early Silurian zircons, the Late

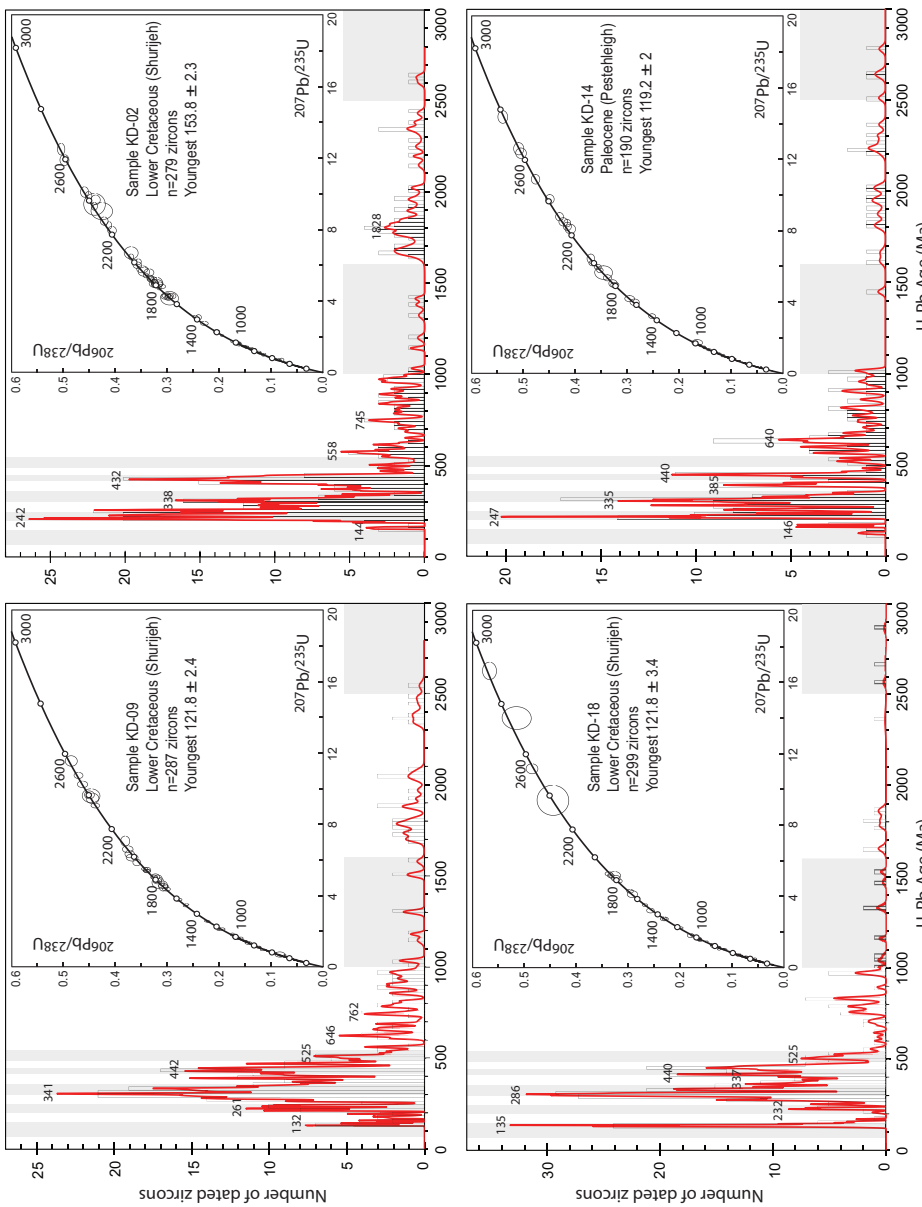

Fig. 8. Detrital zircon $^{206}Pb/^{238}U$ age population probability density diagrams with corresponding Concordia plots for Early Cretaceous and Paleocene samples KD-02, KD-09, KD-14 and KD-18. Ages with discordance greater than 5% are excluded. Time scale after Gradstein and others (2012).

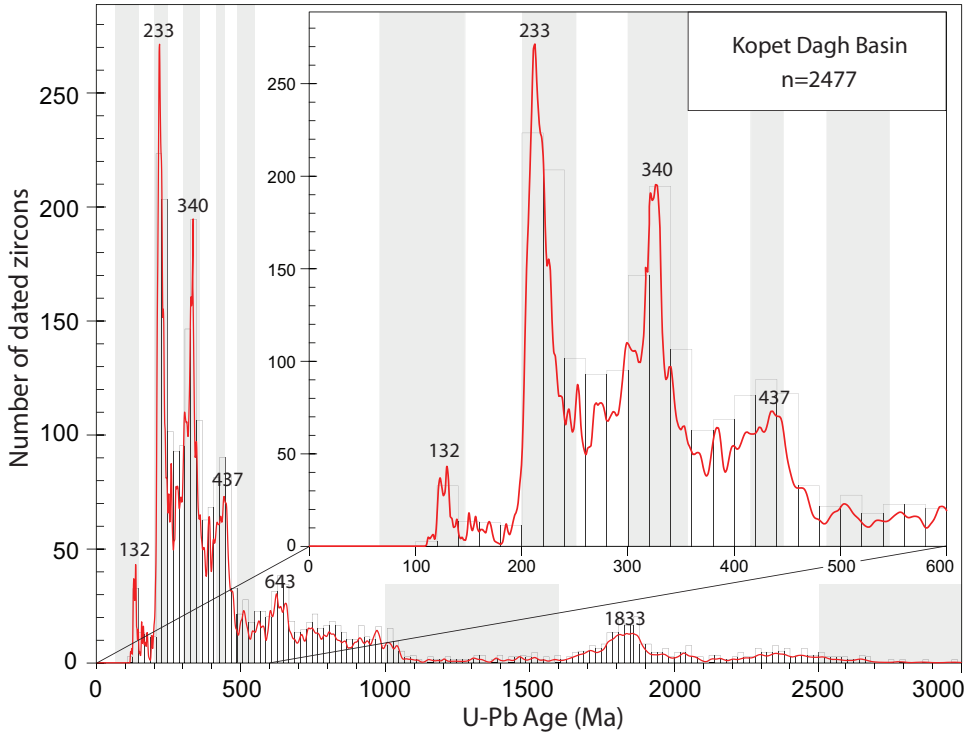

Fig. 9. Combined zircon U-Pb age distribution pattern of Kopet Dagh sandstone samples.

Triassic zircons show mixed positive and negative ε-$Hf_{(t)}$ values from -3 to +7 with one outlier of -15. The only analysed Early Cretaceous zircon shows a ε-$Hf_{(t)}$ value of +7.6 (fig. 11).

DISCUSSION

The presented multi-proxy study of Triassic to Palaeocene sandstones from the Kopet Dagh mountains refine our understanding of the corresponding sediment sources and allows for an improved reconstruction of the tectono-sedimentary evolution of the tectonically inverted Kopet Dagh Basin.

Evidence from Sandstone Framework Compositions

The sandstone modal framework analysis of the sandstone lens within a Triassic polymathic conglomerate (Qara-Gheitan Formation) suggest a transitional magmatic arc provenance (fig. 4C and D). Petrographic analyses on the Qara-Gheitan sandstones by Ghaemi (2009) specify provenance from a dissected magmatic arc. Additionally, geochemical analysis of large granodiorite and tonalite pebbles of the Qara-Gheitan conglomerate by Zanchetta and others, (2013) suggests an active margin setting with prevailing of I-type plutonic and high-K volcanic rocks.

The mineralogical composition of Middle Jurassic sandstones of the Kashafrud Formation composed of sedimentary and volcanic lithic fragments with subordinate metamorphic lithics (fig. 4D) suggest a provenance from a dissected magmatic arc (fig. 4C and D). Modal framework and a SW-NE directed paleocurrent along with stratigraphic studies of Middle Jurassic sandstones by Poursoltani and others (2007)

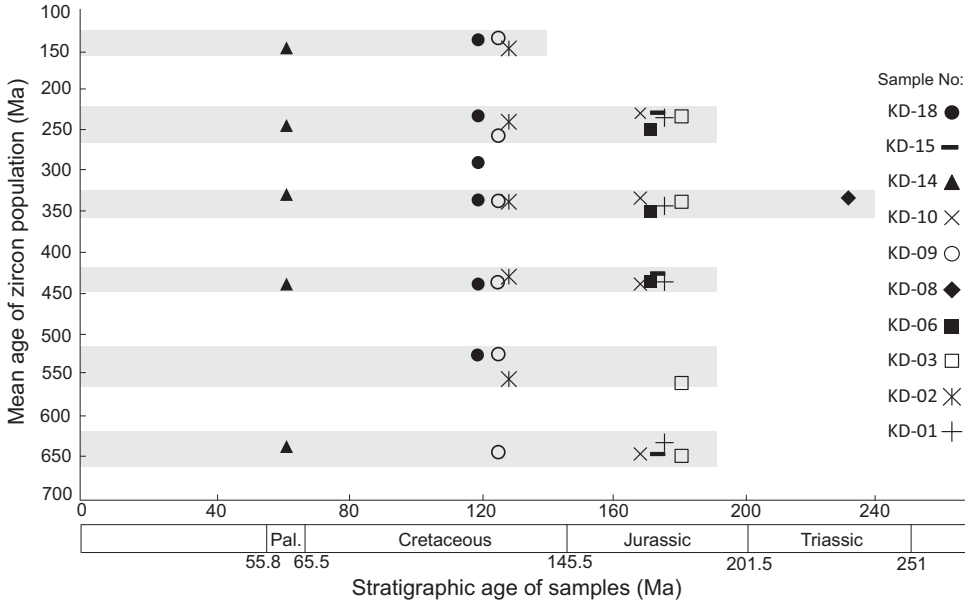

Fig. 10. Detrital zircon U-Pb mean age populations versus stratigraphic age of the Kopet Dagh sandstones. Time scale after Gradstein and others (2012).

and Poursoltani and Gibling (2011) are in agreement with a magmatic arc source. In addition, they suggested that the detritus was supplied from an active margin in the southeast to the extensional Kopet Dagh Basin in the northwest through channel systems to slope and basin-floor fans forming fluvial (basal conglomerate), deltaic (sandstone), and proximal to distal turbiditic (sandstone and mudstone) facies.

Lower Cretaceous sandstones (Shurijeh Formation) show a higher amount of monocrystalline quartz and a lower amount of polycrystalline quartzcompared to Middle Jurassic sandstones (fig. 4B) indicating recycling of older sediments. In addition, modal framework analysis by Mortazavi and others (2013) on Lower Cretaceous sandstones supports a provenance characterized by a recycled signature. Paleocurrent directions of Lower Cretaceous sandstones suggest that sediments were supplied from the south and southwest into the Kopet Dagh Basin (Moussavi-Harami and Brenner, 1990). Therefore, Jurassic sandstones represent a potential source for second-cycle Lower Cretaceous sandstones. Paleocene continental sandstones (Pestehleigh Formation) show a relativly higher content of monocrystalline quartz and a lower content polycrystalline quartz compared to Triassic-Jurassic sandstones (fig. 4B), indicating a recycled provenance (fig. 4C and D). This interpretation agrees with findings of Moussavi-Harami (1993), who suggested that northward and northwestward thinning of coarse-grained Paleocene sandstone layers indicates that the detritus was supplied from the recycling of older sediments in the south and southeast.

Evidence from Heavy Mineral Assemblages

The heavy mineral assemblage of the Triassic sandstone with dominant clinopyroxene minerals (fig. 5 and table 3) indicates a source from mafic magmatic rocks in form of a magmatic arc or even anorogenic continental-flood basalts (Garzanti, 2016), which is in concordance with sandstone modal framework results (fig. 4C and D). In addition, the internal textures (CL images) and Th/U ratios of detrital zircons

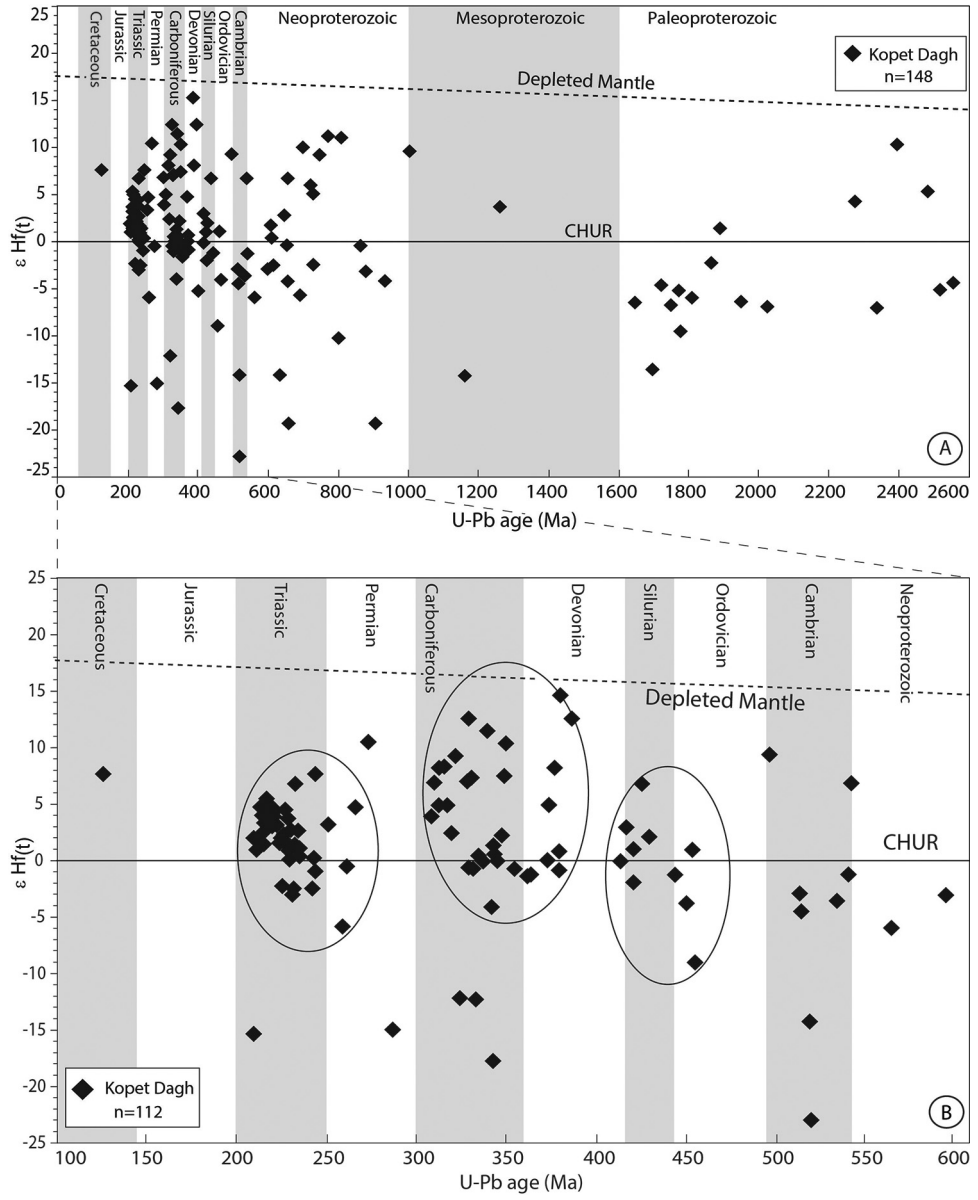

Fig. 11. Time-corrected ϵ-$Hf_{(t)}$ values versus $^{206}U/^{238}Pb$ ages of Kopet Dagh detrital zircons. Depleted mantle evolution trend (dashed line) from Griffin and others (2000), and Chondritic Uniform Reservoir values (CHUR) from Bouvier and others (2008).

from pebbles of the Triassic conglomerate suggest a magmatic origin for these zircons (Zanchetta and others, 2013). An increase in ZTR minerals along with a decreasing percentage of pyroxene minerals in the heavy mineral fraction of Jurassic sandstones (fig. 5 and table 3) imply second-cycle sandstone formed by erosion of pyroclastic-volcanoclastic rocks deposited into a deep-marine basin (Poursoltani and others, 2007). However, the effect of chemical weathering in the decrease of pyroxene as a labile detrital mineral cannot be discarded (Garzanti, 2017).

A significant increase of clastic sedimentary lithics compared to the Triassic sandstone and first appearance of garnets in Jurassic sandstones (fig. 5 and table 3) point toward metamorphic rocks as a minor additional source of detritus. Poursoltani and Gibling (2011) reported ZTR minerals along with apatite and garnet as the main heavy mineral spectrum in the Jurassic sandstones, coinciding with our findings. Lower Cretaceous sandstones indicate a high percentage of ZTR minerals and Cr-spinel, and a reduced quantity of pyroxene minerals in the heavy mineral assemblages. The amount of pyroxene (20%) in Jurassic sandstones decreases to 1.5% in Cretaceous sandstones (fig. 5 and table 3). This indicates that the heavy mineral content was partly controlled by recycling of older sandstones. An increase of monocrystalline quartz content along with a decrease of less stable volcanic lithics in Lower Cretaceous sandstones compared to older lithologies provides further evidence for recycling of Jurassic sandstones (table 3). In addition, Poursoltani and Gibling (2011) and Mortazavi and others (2013) suggested a moderate weathering in source areas before deposition based on alteration of volcanic rocks and ferromagnesian minerals in Jurassic sandstones and geochemical analysis of Early Cretaceous sandstones.

The main diagenesis features of the Jurassic and Early Cretaceous sandstones (Kashafrud and Surijeh formations) are compaction, pressure solution of carbonates, cementation (carbonate, rarely dolomite and iron oxides), burial alteration of ultrabasic and ferromagnesian minerals, authigenic mineral formation (K-feldspar, albite and clay minerals), and dissolution (Moussavi-Harami and Brenner, 1993; Poursoltani and Gibling, 2011; Mortazavi and others, 2014). This indicates the effect of diagenesis on the partial dissolution of less-durable heavy minerals. However, the oversized, cement-filled pores that might indicate total dissolution of framework grains are absent in Kopet Dagh sandstones (Poursoltani and Gibling, 2011). This indicates a relatively low effect of diagenesis on heavy minerals variation in the Kopet Dagh sandstones.Paleocene sandstones indicate a heavy mineral spectrum similar to the one of Lower Cretaceous sandstones. However, the amount of garnet increases from 3.5% in Lower Cretaceous sandstones to 15.5% in Paleocene sandstones. This implies that erosion of garnet-bearing metamorphic rocks, along with recycling of the older sandstones, were the main sources of detritus in the Palaeocene. The most probable source of garnet and metamorphic lithic grains are Carboniferous-Permian metamorphic rocks to the southeast of the Kopet Dagh Basin (figs. 2 and 3).

Evidence from Detrital Zircon U-Pb Ages and Hf Isotopes

The 2477 analyzed detrital zircon grains from the Lower Triassic, Middle Jurassic, Lower Cretaceous, and Paleocene turbiditic, deltaic-fluvial, and continental sandstones yielded apparent ages ranging from *ca.* 119 Ma to *ca.* 2966 Ma (figs. 7, 8, 9 and 10). Six major U-Pb age groups are identified.

Mesoarchean to Paleoproterozoic zircons

The oldest zircons create a broad heterogeneous age spectrum from Mesoarchean to Paleoproterozoic (2966–1600 Ma) with a main peak in the Paleoproterozoic (1833 Ma; fig. 9), containing ~11% of total dated zircons, characterized by anhedral to rounded grains without internal zoning (>80%), and a wide range of Th/U ratios (between 0.01 and 2.39; fig. 6 and table S4). The ε-$Hf_{(t)}$ values of Mesoarchean to Early Paleoproterozoic zircons represent a mixture of positive and negative values (-6.9 to +10.3), while Late Paleoproterozoic zircons show dominantly negative values (-13.6 to -2.3) with only one grain of positive value (+ 1.4; fig. 11 and table S6). Possibly, these are inherited magmatic zircons or fragments of older reworked zircons from metamorphic/igneous source areas that remain undefined due to repetitive reworking through several tectonic cycles since the Archean. However, similar age spectra with a major peak at

2.5 Ga and a minor peak at 1.8 Ga were reported in Neoproterozoic to Cambrian, Lower Permian and Middle Jurassic, and Devonian sandstones of the Alborz mountains (Horton and others, 2008; Moghadam and others, 2017; Zoleikhaei and others, 2021). Mesoarchean to Paleoproterozoic zircons were furthermore reported in Cretaceous to Eocene sandstones of Azerbaijan Basin (Mohammadi and others, 2022), Eocene to Oligocene sandstones from the Sistan Basin (Mohammadi and others, 2016a), Cretaceous to Miocene sandstones of the Makran Basin in Iran (Mohammadi and others, 2016b; 2017), Palaeozoic sandstones of Wajid and Tabuk area in Saudi Arabia (Meinhold and others, 2020), and Paleozoic to Triassic sandstones of the Taurides mountains in Turkey (Abbo and others, 2015). There are no reported occurrences of Archean to Paleoproterozoic zircons in the Iranian or Anatolian continental crust (for example, Ramezani and Tucker, 2003; Moghadam and others, 2017; Moghadam and others, 2020). However, Archean to Paleoproterozoic zircons with similar peaks were identified from Tibetan terranes including Songpan Ganzi (Weislogel and others, 2006) and Nan Shan-Qilian Shan-Altun Shan (Gehrels and others, 2011), and the Tarim craton (Gehrels and others, 2011). The lack of a 1.8 Ga and presence of a 1.9 Ga zircon age peak in the Archean to Paleoproterozoic age spectrum of Iberia and African Neoproterozoic to Cambrian sandstones (Abdelsalam and others, 2002) excludes the Saharan meta-craton as a potential source area. In fact, the source of Archean to Paleoproterozoic zircons in the Kopet Dagh strata remains enigmatic. Zoleikhaei and others (2021) suggested the basement terranes of the Arabian-Nubian Shield as a plausible source of Mesoarchean to Paleoproterozoic detrital zircons of the Alborz Cambrian sandstones, which could also be the case for the Kopet Dagh Basin. (fig. 10).

Neoproterozoic zircons

The second age population includes Neoproterozoic detrital zircons (1000–542 Ma) show a main peak at 643 Ma (fig. 9), including ~18% of the total dated zircons. Neoproterozoic zircons are mostly rounded or anhedral grains with sporadic magmatic or metamorphic growth zoning or no zoning (fig. 6). Neoproterozoic zircons show Th/U ratios with a wide range between 0.01 and 2.92 (table S4), which indicate both magmatic and metamorphic ultimate sources. Due to different grain shapes and internal growth structures, these zircons are probably remnants of older recycled grains or inherited cores from continental crystalline rocks. The ε-$Hf_{(t)}$ values of Neoproterozoic zircons range between -19.3 and +11.3 (fig. 11 and table S6). Neoproterozoic (Pan-African) detrital zircons were reported from several Gondwana-related tectono-stratigraphic domains such as Iran (for example, Ramezani and Tucker, 2003; Hassanzadeh and others, 2008; Hosseini and others, 2015), the Taurides (Abbo and others, 2015), Libya (Meinhold and others, 2013), the Arabian-Nubian Shield (Morag and others, 2012), and north Africa (Abati and others, 2010; Avigad and others, 2012). Furthermore, detrital zircons with a main peak at 660–620 Ma were reported from Early Cambrian sandstones of the Alborz Mountains (Zoleikhaei and others, 2021). Indicative for Neoproterozoic zircons is the lack of 600–520 Ma old grains, which marks a widespread period of intense magmatism in Central Iran, excluding the latter as a suitable source of Kopet Dagh strata during these times, and rather supports repetitive recycling of the Cryogenian to Ediacaran crystalline basement of the Arabian-Nubian Shield to be the ultimate source (fig. 10).

Ordovician to Silurian zircons

The third age group denotes Ordovician to Silurian zircons (465–422 Ma) with a peak at 437 Ma (~9.3% of total dated zircons) exhibit subhedral to euhedral shapes, dominantly magmatic zoning, and Th/U ratios above 0.5 (fig. 6 and table S4), indicating an abundant magmatic source. ε-$Hf_{(t)}$ values (-1.9 to +6.7, only one grain with

-8.9; fig. 11 and table S6) suggest a juvenile source with a mantel signature. Presented zircon ages correspond to major rifting episodes that occurred from Late Ordovician to Silurian along the northern Gondwana margin (Gaetani 1997; Stampfli, 2000; Moghadam and others, 2020), which correspond to the separation of the Hun terranes from Gondwana along with the opening of Paleo-Tethys Ocean (Moghadam and others, 2020). Late Ordovician to Middle Silurian rift-related magmatism was furthermore reported from northern Central Iran (for example, Nowrouzi and others, 2014), eastern Alborz (Derakhshi and Ghasemi, 2015; Moghadam and others, 2020), and Anatolia (for example, Topuz and others, 2020, 2021). In the eastern Alborz, Silurian basaltic and basaltic-andesitic magmatism occurred (local name: Soltan Maidan Complex; Ghavidel-Syooki and others, 2011; Derakhshi and Ghasemi, 2015), however, these rocks are not expected to have provided an important zircon input. The geochemistry of this volcanic units shows alkaline affinity with an intra-plate and continental-rift setting (Derakhshi and Ghasemi, 2015). The zircon U-Pb ages of rounded granitic pebbles from conglomerate layers at the base and in the middle of the aforementioned volcanic unit indicate an Early Silurian crystallization age (434 ± 6.4 Ma; Ghavidel-Syooki and others, 2011). Furthermore, zircon U-Pb ages of A-type granitic pebbles from Devonian sandstones (Padeha Formation) in the eastern Alborz indicate Early Silurian ages (441 ± 3.1 Ma) with $\varepsilon Hf_{(t)}$ values ranging from +8.2 to +2.5 (Moghadam and others, 2017). The zircon U-Pb age of granitic pebbles from both Silurian and Devonian successions fit well with the main peak (437 Ma) of the Late Ordovician to Silurian detrital zircon population of the Kopet Dagh sandstones (fig. 9). Furthermore, Ordovician to Silurian detrital zircons with a main peak at 435 Ma and $\varepsilon Hf_{(t)}$ values of -3.6 to +6.3 from Late Ordovician (Qelli Formation) sandstones from eastern Alborz were reported by Moghadam and others (2017). Taking into consideration all above-mentioned criteria as well as a short transport distance between eastern Alborz and Kopet Dagh, the Ordovician to Silurian detritus of the Kopet Dagh Basin was most probably supplied through recycling of Ordovician to Devonian sandstones from the eastern Alborz.

Devonian to Carboniferous zircons

The forth age population (385–305 Ma) with a main peak at 340 Ma (fig. 9) exhibits dominantly euhedral zircon grains (~75%) with magmatic internal texture and high Th/U ratios (> 0.5; fig. 6 and table S4). This age spectrum comprises ~17% of the total analyzed detrital zircons (table S4). $\varepsilon\text{-}Hf_{(t)}$ values range between -1.4 and +15.3 with three grains between -12.1 and -17.7 (fig. 11 and table S6), in average broadly chondritic with a juvenile component (Patchett, 1983; Blichert-Toft and Albarède, 1997). Carboniferous detrital zircons with a main peak at 344–347 Ma from Cretaceous turbiditic sandstones of Azerbaijan (NW Iran) were reported by Mohammadi and others (2022). However, a potential source area includes the northeast of Iran, where Devonian to Carboniferous meta-sedimentary and magmatic rocks were reported from the Aghdarband complex (Zanchetta and others, 2013; Moghadam and others, 2015a). The age of metasedimentary rocks in the north of Aghdarband complex (Behrouzi and others, 1993; Zanchetta and others, 2013) provides an indirect clue of basement age of this complex. Age constraints for Aghdarband complex include zircon U-Pb ages of plagiogranite dikes and ferro-diorites (382–380 Ma) from the Darrehanjir ophiolites indicatıng a Late Devonian age (Moghadam and others, 2015a) and zircon U-Pb ages of granitoid cobbles in the Qara-Gheitan conglomerate indicate giving a Late Carboniferous (314 Ma) age (Zanchetta and others, 2013). The wide range of Devonian to Carboniferous sedimentary and igneous rocks in the Aghdarband complex is in concordance with detrital zircon ages distributions in the Kopet Dagh sandstones (fig. 9). Furthermore, the Paleo-

Tethys continental arc along the southern margin of the Aghdarband complex and widespread Late Paleozoic to Early Mesozoic volcanism in the Turan Block reported by Natalin and Şengör (2005) could represent another possible source for Early Carboniferous detrital zircons from the Kopet Dagh. However, the reported general SE-NW paleocurrent direction in the Kopet Dagh sandstones (Poursoltani and others, 2007) strengthen the case that the Devonian to Carboniferous detritus was supplied from the Aghdarband complex and the Paleo-Tethys continental arc rather than from the Turan Block.

Permian to Triassic zircons

The fifth zircon age spectrum in the Kopet Dagh sandstones (300–200 Ma) show a peak at 233 Ma (fig. 9) and incorporate ~25.4% of the total dated zircons (table S4) exhibiting euhedral shapes (>80%) with magmatic zoning (fig. 6). Furthermore, over 90% of zircons in this spectrum indicate a high Th/U ratio (>0.55; table S4), which denotes a magmatic origin. $\varepsilon\text{-Hf}_{(t)}$ values of Permo-Triassic zircons range between -5.9 and +10.3 (>80%) with two grains with values of -15 and -15.2 (fig. 11 and table S6). The mixed positive and negative $\varepsilon\text{-Hf}_{(t)}$ values of the Permo-Triassic zircons propose juvenile source (plausibly the depleted mantle) and a more evolved crustal source in a continental magmatic arc (Patchett, 1983; Blichert-Toft and Albarède, 1997). Both Permian and Triassic ages were reported from the Fariman and Mashhad complexes in the south of the Kopet Dagh Basin, representing potential source areas (for example, Karimpour and others, 2010; Mirnejad and others, 2013; Zanchetta and others, 2013; Moghadam and others, 2015a; Chiu and others, 2017; Topuz and others, 2018).

The late Early Permian to Middle Permian Fariman complex consists of ta lower metamorphosed unit and an upper volcanic-sedimentary unit (Zanchetta and others, 2013). The ^{40}Ar-^{39}Ar dating of hornblende from olivine cumulates yielded Early Permian (276 ± 4 Ma) ages (Topuz and others, 2018) and andesitic dikes dated at 211 Ma indicate Late Triassic magmatic activity (Zanchetta and others, 2013). The Fariman complex has been interpreted as a continental magmatic arc with an intra-arc basin (Zanchetta and others, 2013), a subduction- and plume-related Paleo-Tethyan ophiolite (Moghadam and others, 2015a), as well as a fragment of an oceanic plateau (Topuz and others, 2018).

The Mashhad Complex (fig. 2) represents a remnant of the Paleo-Tethys oceanic crust and includes three members: i) The lower ophiolite member with Early Permian age (^{40}Ar-^{39}Ar ages of hornblende from gabbros: 287.6 Ma and 281.7 Ma; Ghazi and others, 2001). ii) The Middle Permian-Triassic deep-water turbidites (accretionary prism). iii) The upper arc-related pyroclastic rocks (Moghadam and others, 2015a). Post-collisional intrusive bodies with granitoid and monzogranite suites (U-Pb zircon ages between 200 and 217 Ma) crosscut the Mashhad complex (Karimpour and others, 2010; Mirnejad and others, 2013). Additionally, the Mashhad granodiorite and diorite were dated to 203 Ma and 219 Ma, respectively, showing $\varepsilon\text{-Hf}_{(t)}$ values between -3 to +3 (Chiu and others, 2017). The southeastward continuation of the Mashhad Complex (Torbat-e-Jam Complex) was intruded by post-collisional I-type granitites (217 Ma; Zanchetta and others, 2013) and gabbro-quartz diorite (215 Ma; Ghavi and others, 2018) of similar ages. According to Zanchetta and others (2013), the age range of post-collisional intrusions indicates that the obduction of the Mashhad ophiolites occurred before the Late Triassic (Norian-Rhaetian).

The age spectrum and dominant positive $\varepsilon\text{-Hf}_{(t)}$ values of Permian to Triassic zircons and the presence of first-cycle chromium spinel in the heavy mineral assemblage of Triassic and Lower Jurassic sandstones indicates an exposure of mafic-ultramafic rocks in the source area (Garzanti and Andò 2019). This interpretation is in

agreement with unroofing and consequent deposition of the Mashhad and Fariman complexes, and a remnant of Triassic continental arc in the Kopet Dagh Basin. Northward directed paleocurrents and the presence of Norian granodiorite pebbles (211 Ma) in the conglomerate underlying Jurassic sandstones indicate erosion and unroofing of post-collisional intrusive bodies and ophiolitic host rocks south of the Kopet Dagh Basin in the Middle Jurassic time (for example, Zanchi and others, 2009; Zanchetta and others, 2013; Zanchi and others, 2016).

Early Cretaceous zircons

The sixth and youngest age population (146–119 Ma) with a main peak at 132 Ma (fig. 9) contains only 1.5% of the total dated zircon grains (able S4). Zircon grains are euhedral in shape, exhibit magmatic zoning, and show Th/U ratios >0.3 (fig. 6 and table S4). ε-$Hf_{(t)}$ values of +7.6 indicate non-depleted mantle signatures (fig. 11 and table S6). Occurrence of Early Cretaceous zircons in Lower Cretaceous sandstones (samples KD-09 and KD-18) and the Paleocene sandstone (sample KD-14; figs. 8 and 10) indicate minor syn-sedimentary magmatic activity in the source area. Furthermore, the presence of detrital zircons with Early Aptian ages (~124 Ma; average of 8 youngest ages) in Lower Cretaceous sandstones of the Shurijeh Formation indicate maximum depositional ages younger than the previously reported Neocomian stratigraphic age (for example, Afshar-Harb 1982a, 1982b; Afshar-Harb and others, 1986; Behrouzi and others, 1993; Moussavi-Harami and Brenner, 1993; Mortazavi and others, 2014). A potential source area of Early Cretaceous zircons is the Cheste Sharif pluton located in the Band-e-Bayan Zone (a narrow W-E trending crustal block bounded by the large-scale Hari Rod fault, northern Afghanistan), which is dated at 138 Ma by K-Ar biotite (Debon and others 1987). The presence of Early Cretaceous zircons in Lower Cretaceous sandstones in the eastern Kopet Dagh (fig. 2) is in agreement with a detritus supply from the Band-e-Bayan Zone during Early Cretaceous time. Most probably, Early Cretaceous zircons in the Paleocene sandstones were recycled from Lower Cretaceous sandstones of the Kopet Dagh Basin (fig. 10).

REGIONAL TECTONIC IMPLICATIONS

Integrated provenance analysis including zircon ages and isotopic compositions of the Mesozoic to Paleocene detrital material in the Kopet Dagh Basin recorded three main tectonic events in the Phanerozoic (figs. 9 and 11). These events took place in Late Ordovician to Early Silurian (main peak at 437 Ma), Late Devonian to Early Carboniferous (main peak at 340 Ma), and Late Permian-Triassic (main peak at 233 Ma). The first event (Late Ordovician to Early Silurian) corresponds to the separation of Eurasia from Gondwana and the consequent opening of the Paleo-Tethys Ocean (for example, Stampfli and Borel, 2002; Stampfli and others, 2013) (fig. 12; 440 Ma). This rifting event is marked by mafic magmatism along the northern margin of Gondwana (Alborz Mountains; Derakhshi and Ghasemi, 2015), and is in agreement with Hf-isotopic composition (juvenile source with mantel signature) of Ordovician-Early Silurian detrital zircons of the Kopet Dagh Basin.

The second recorded event in Late Devonian to Early Carboniferous coincides with a plutonic episode with A-type (intra-continental) magmatism in NW Iran (Azerbaijan area) and the Sanandaj-Sirjan Zone (for example, Mohammadi and others, 2020). In addition, Late Devonian to Early Carboniferous ages are represented by a series of mafic and ultramafic rocks (ophiolites and oceanic igneous complexes) from Turkey in the west to Tibet to the east (for example, Moghadam and others, 2015b). This event records the first stages of Paleo-Tethys subduction beneath the Turan Block that initiated in Late Devonian (~380 Ma) and continued until the Late Triassic (Moghadam and others, 2015a) (fig. 12; 380 Ma). According to Zanchetta

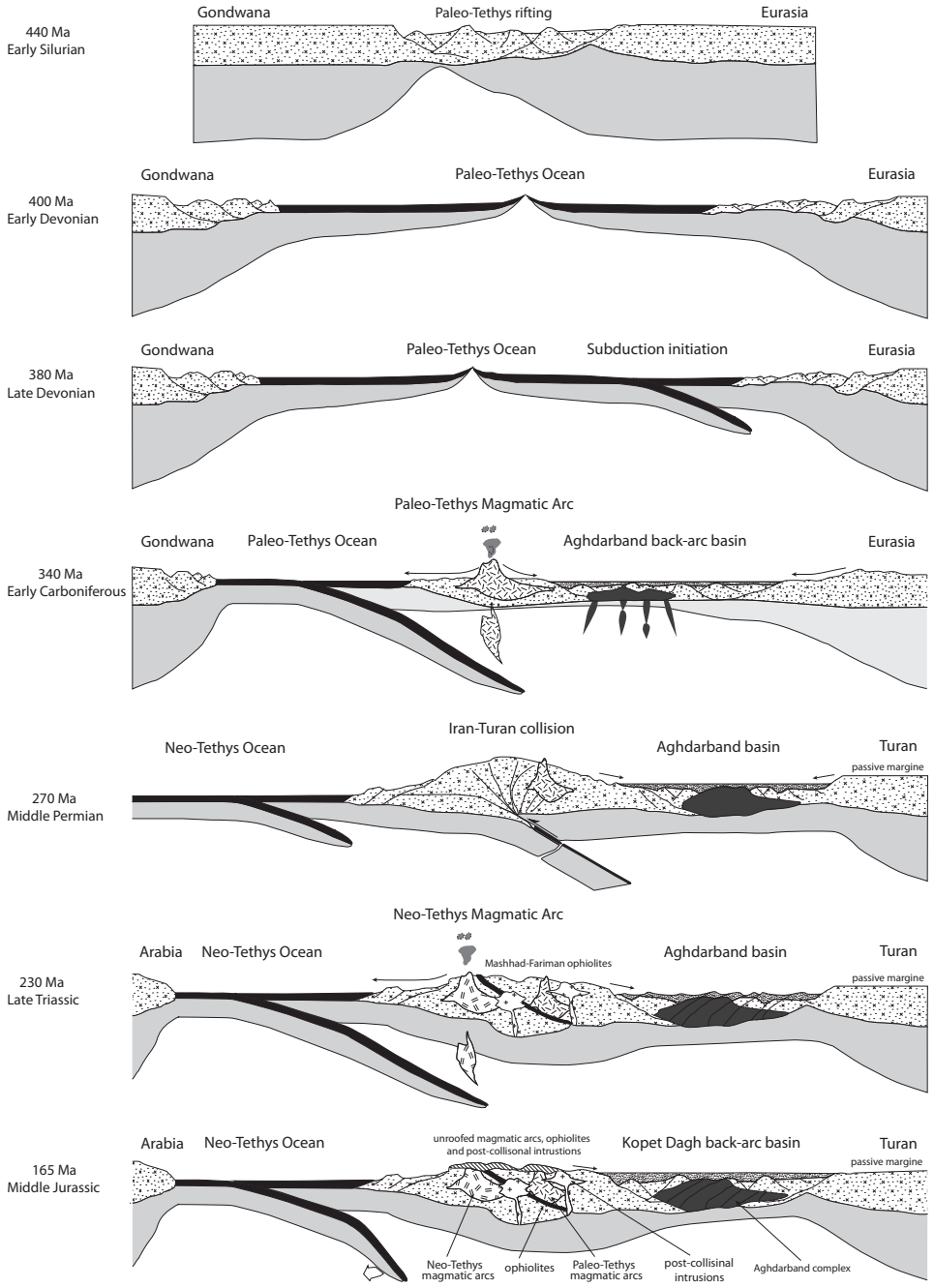

Fig. 12. Tectonic reconstruction along N-S profiles of the Kopet Dagh Basin from Early Silurian to Middle Jurassic.

and others (2013), the exposed Devonian to Carboniferous Aghdarband and Permo-Triassic Fariman complexes in NE Iran formed as a back-arc and an intra-arc basin, respectively, along the southern margin of the Turan Block, and related volcaniclastic

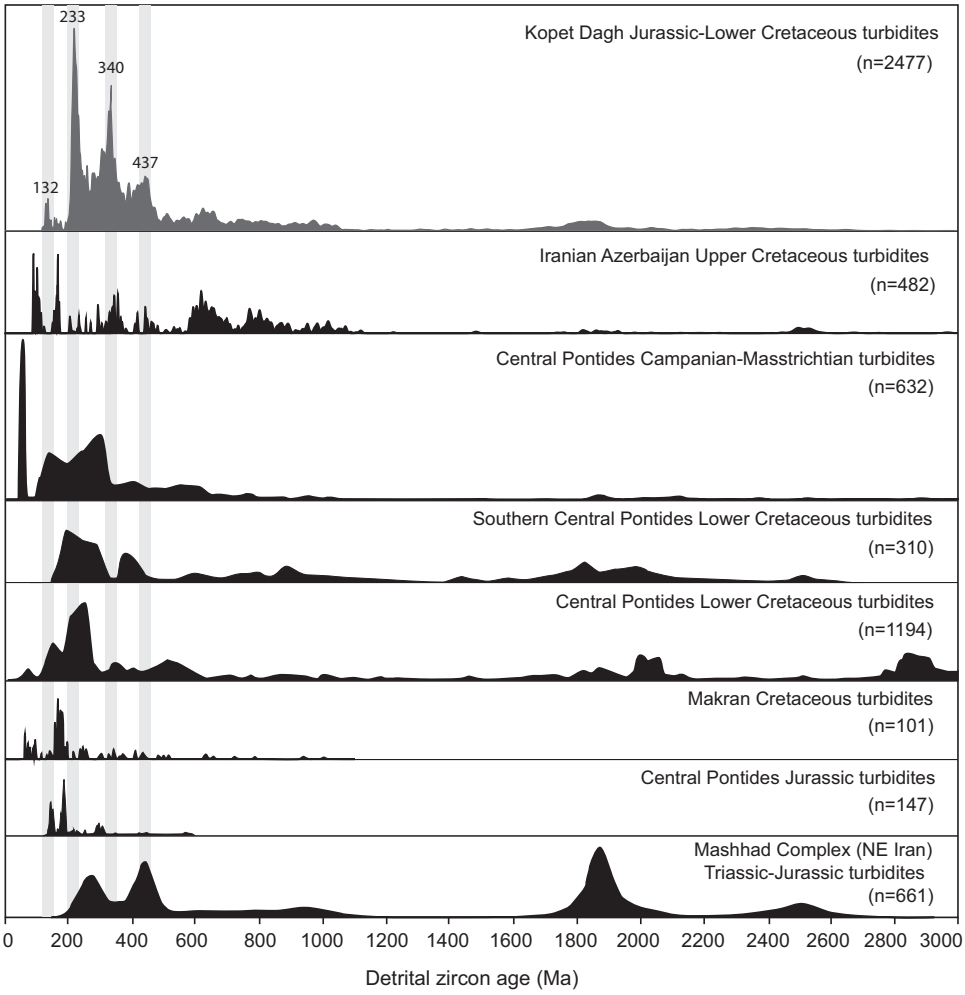

Figure 13. Normalized probability plots of detrital zircon distribution pattern of Mesozoic strata of Turkey and Iran: Mashhad Complex (NE Iran) Triassic-Jurassic turbidites (Chu and others, 2021); Central Pontides Jurassic turbidites (Akdoğan and others, 2018); Makran Cretaceous turbidites (Mohammadi and others, 2016b); Central Pontides Lower Cretaceous turbidites (Akdoğan and others, 2017); Southern Central Pontides Lower Cretaceous turbidites (Okay and others, 2013); Central Pontides Campanian-Masstrichtian turbidites (Akdoğan and others, 2019), and Iranian Azerbaijan Upper Cretaceous turbidites (Mohammadi and others, 2022).

rocks were supplied from an active magmatic arc in the south of the Kopet Dagh Basin (fig. 12; 340 Ma). Contrariwise, Moghadam and others (2015a) argued that the Aghdarband and Mashhad ophiolites in NE Iran were part of the Paleo-Tethys oceanic crust, where related volcanoclastic rocks were supplied from an active magmatic arc (Silk Road Arc) in the north of the Kopet Dagh Basin. The SW-NE paleocurrent direction and new zircon data presented in this study with the main peak at 340 Ma support the hypothesis of Zanchetta and others (2013) and point toward intensified rifting and spreading of a back-arc basin ~40 Ma after the initiation of the Paleo-Tethys subduction (fig. 12; 380 Ma).

The third event coincides with a Permian-Triassic continental magmatic arc that formed during the northward subduction of the Paleo-Tethys Ocean beneath the

Turan (Eurasia) plate and the subsequent Late Triassic (Norian-Rhaetian) continental collision (fig. 12; 230 Ma). The Mashhad Ophiolite Complex was obducted onto the Iranian microcontinent in early Late Triassic (Carnian-Norian; Moghadam and others, 2015b). Finally, collision between the Iran and Turan plates occurred in Late Triassic (Norian-Rhaetian) and was accompanied by the intrusion of several post collisional plutonic bodies into the magmatic arc and the Mashhad Ophiolite Complex (fig. 12; 230 Ma). Finally, unroofing of the magmatic arc, the Mashhad Ophiolite Complex, and related post-collisional intrusions in Middle Jurassic led to deposition of Middle Jurassic turbiditic sandstones in the Kopet Dagh extensional basin (fig. 12; 165 Ma). A compilation of detrital zircon U-Pb age distribution patterns of Jurassic-Cretaceous strata of the Kopet Dagh and other mountain belts along the Arabia-Eurasia plate boundary allow for a comparison of primary, or an identification of secondary potential source areas (fig. 13). Such a comparison may help reconstructing paleo-geographic connections between contemporaneous sedimentary basins along the northern Gondwana margin during the Mesozoic. Ordovician to Silurian detrital zircons (peak at 437 Ma in the Kopet Dagh) indicating Gondwana-related rifting (for example, Nowrouzi and others, 2014; Derakhshi and Ghasemi, 2015; Moghadam and others, 2020; Topuz and others, 2020, 2021) were also detected in Mesozoic turbidites of the Mashhad complex and to a lesser degree in Upper Cretaceous turbidites from the Iranian Azerbaijan, but are not indicative for the Makran strata to the south nor for turbidites from the northern Turkish Pontides farther to the west (fig. 13). This indicates that most probably, the timing of Paleo-Tethys rifting of the Turkish segment was not synchronous with the Iranian segment.

Devonian to Carboniferous zircon ages (peak at 340 Ma in Kopet Dagh strata) can also be found in Upper Cretaceous turbidites from Iranian Azerbaijan, but are absent in other Mesozoic strata, except for a minor peak in Lower Cretaceous rocks of the Central Pontides (fig. 13). The absence of a Devonian-Carboniferous age peak in zircons from the Triassic-Jurassic Mashhad Complex (Paleo-Tethys oceanic crust; Chu and others, 2021) supports that the Aghdarband complex was separated from the Paleo-Tethys to the south. In the Middle Jurassic, the Kopet Dagh likely opened as a back-arc basin to the Neo-Tethys by reactivating an inherited back-arc basin to the Paleo-Tethys subduction represented by igneous and sedimentary rocks of the Aghdarband complex (Zanchetta and others, 2013; Zanchi and others, 2016). The Jurassic-Cretaceous basin extended westward along the Caspian and Greater Caucasus (Brunet and others, 2003) reaching at least northwestern Iran, where a similar age peak is found (fig. 13). This age constraint is synchronous with the final closure of the Turkish segment of the Rheic Ocean and the collision of Pontides-Trans Caucasus Block with Baltica (for example, Hanel and others, 1992; Allen and others, 2006).

Triassic zircons of Kopet Dagh Jurassic-Cretaceous sequences with a peak at 340 Ma show post-collisional intrusive bodies as main source. These post-collisional granitoids intruded into the Mashhad and Fariman complexes after the final collision of Central Iran and Eurasian plates in NE Iran. Contrariwise, Triassic zircons are almost absent in Mesozoic strata from Iranian Azerbaijan (fig. 13). A possible reason for this discrepancy is the extension of the Khoy Ocean into Iranian Azerbaijan as a subordinary arm of the Neo-Tethys Ocean (Lechmann and others, 2018). This explains the different evolutional history and sediment source areas for the Iranian and Turkish segments of the Neo-Tethys ocean.

CONCLUSIONS

The present study tentatively assesses the provenance of detrital sediments in Triassic to Paleocene turbiditic, fluvial-deltaic and continental sandstones of the Kopet Dagh Basin in northeast Iran. Over 2470 detrital zircons U-Pb ages yield a

spectrum of variable protoliths from Archean to Early Cretaceous (2966–119 Ma) with main peaks in Paleoproterozoic (1883 Ma), Neoproterozoic (643 Ma), Early Silurian (437 Ma), Early Carboniferous (340 Ma), Late Triassic (233 Ma), and a minor peak in Early Cretaceous (132 Ma). The combined U-Pb ages and Hf isotope data indicate that protolith rocks belonged to an Early Silurian intracontinental rift (opening of Paleo-Tethys), an Early Carboniferous rifting of a back-arc (Aghdarband Complex), and a Late Triassic collisional to post-collisional (Paleo-Tethys collision) magmatism. Our results highlight the timing of the Aghdarband Complex formation as a back-arc basin ~40 Ma after subduction initiation of the Paleo-Tethys. The Middle Jurassic Kopet Dagh Basin likely reactivated back-arc extension, now driven by the newly established Neo-Tethys subduction to the south. Cr-spinel and heavy mineral assemblages imply additional detritus sourcing from exhumed ophiolites (Mashhad and Fariman complexes). Our analytical results furthermore suggest that the majority of Jurassic sedimentary detritus sourced from protoliths in the south of the Kopet Dagh Basin and deposited in a submarine fan-delta complex. In the Early Cretaceous detritus was supplied from similar protoliths and furthermore from recycled Jurassic turbiditic sandstones. These sediments were deposited in a fluvial-deltaic complex. The Paleocene continental sediments were mainly supplied from recycling of exposed Jurassic to Early Cretaceous sediments.

ACKNOWLEDGMENTS

The work supported by the Swiss National Science Foundation (grant no. 200021-153124/1). We thank the National Iranian Oil Company for logistic support during field trips. Invaluable comments by Eduardo Garzanti and Jack Mulder considerably improved the paper. We thank Peter Cawood for efficient editorial handling of the manuscript.

SUPPLEMENTARY DATA

https://earth.eps.yale.edu/%7eajs/SupplementaryData/2022/Mohammadi/

REFERENCES

Abati, J., Aghzer, A. M., Gerdes, A., and Ennih, N., 2010, Detrital zircon ages of Neoproterozoic sequences of the Moroccan Anti-Atlas belt: Precambrian Research, v. 181, n. 1–4, p. 115–128, https://doi.org/10.1016/j.precamres.2010.05.018

Abbo, A., Avigad, D., Gerdes, A., and Güngör, T., 2015, Cadomian basement and Paleozoic to Triassic siliciclastics of the Taurides (Karacahisar dome, south-central Turkey): paleogeographic constraints from U–Pb–Hf in zircons: Lithos, v. 227, p. 122–139, https://doi.org/10.1016/j.lithos.2015.03.023

Abdelsalam, M. G., Liégeois, J. P., and Stern, R. J., 2002, The Saharan metacraton: Journal of African Earth Sciences, v. 34, n. 3–4, p. 119–136, https://doi.org/10.1016/S0899-5362(02)00013-1

Afshar-Harb, A., 1982a, Sarakhs geological quadrangle map: National Iranian Oil Company, scale 1:250,000.

Afshar-Harb, A, 1982b, Darreh Gaz geological quadrangle map: National Iranian Oil Company, scale 1:250,000.

Afshar-Harb, A., Aghanabati, A., Shahrabi, M., Davoudzadeh, M., Madjdi, B., and Alavi-Tehrani, N., 1986, Mashhad geological quadrangle map: Geological survey of Iran, scale 1:250,000.

Akdoğan, R., Okay, A. I., Sunal, G., Tari, G., Meinhold, G., and Kylander-Clark, A. R., 2017, Provenance of a large Lower Cretaceous turbidite submarine fan complex on the active Laurasian margin: Central Pontides, northern Turkey: Journal of Asian Earth Sciences, v. 134, p. 309–329, https://doi.org/10.1016/j.jseaes.2016.11.028

Akdoğan, R., Okay, A. I., and Dunkl, I., 2018, Triassic-Jurassic arc magmatism in the Pontides as revealed by the U-Pb detrital zircon ages in the Jurassic sandstones of northeastern Turkey: Turkish Journal of Earth Sciences, v. 27, n. 2, p. 89–109, https://doi.org/10.3906/yer-1706-19

Akdoğan, R., Okay, A. I., and Dunkl, I., 2019, Striking variation in the provenance of the Lower and Upper Cretaceous turbidites in the Central Pontides (Northern Turkey) related to the opening of the Black Sea: Tectonics, v. 38, n. 3, p. 1050–1069, https://doi.org/10.1029/2018TC005119

Alavi, M., 1996, Tectonostratigraphic synthesis and structural style of the Alborz mountain system in northern Iran: Journal of Geodynamics, v. 21, n. 1, p. 1–33, https://doi.org/10.1016/0264-3707(95)00009-7

Alavi, M., Vaziri, H., Seyed-Emami, K., and Lasemi, Y., 1997, The Triassic and associated rocks of the Nakhlak and Aghdarband areas in central and northeastern Iran as remnants of the southern Turanian active continental margin: Geological Society of America Bulletin, v. 109, n. 12, p. 1563–1575, https://doi.org/10.1130/0016-7606(1997)109<1563:TTAARO>2.3.CO;2

Allen, M. B., Ghassemi, M. R., Shahrabi, M., and Qorashi, M., 2003, Accommodation of late Cenozoic oblique shortening in the Alborz range, northern Iran: Journal of Structural Geology, v. 25, n. 5, p. 659–672, https://doi.org/10.1016/S0191-8141(02)00064-0

Allen, M. B., Morton, A. C., Fanning, C. M., Ismail-Zadeh, A. J., and Kroonenberg, S. B., 2006, Zircon age constraints on sediment provenance in the Caspian region: Journal of the Geological Society, v. 163, n. 4, p. 647–655, https://doi.org/10.1144/0016-764920-068

Avigad, D., Gerdes, A., Morag, N., and Bechstädt, T., 2012, Coupled U–Pb–Hf of detrital zircons of Cambrian sandstones from Morocco and Sardinia: implications for provenance and Precambrian crustal evolution of North Africa: Gondwana Research, v. 21, n. 2–3, p. 690–703, https://doi.org/10.1016/j.gr.2011.06.005

Barbarin, B., 1999, A review of the relationships between granitoid types, their origins and their geodynamic environments: Lithos, v. 46, n. 3, p. 605–626, https://doi.org/10.1016/S0024-4937(98)00085-1

Behrouzi, A., Eftekhar-Nezhad, J., and Alavi Naini, M., 1993, Torbat-e-Jam geological quadrangle map: Geological survey of Iran, scale 1:250,000.

Berberian, M., and King, G. C. P., 1981, Towards a paleogeography and tectonic evolution of Iran: Canadian Journal of Earth Sciences, v. 18, n. 2, p. 210–265, https://doi.org/10.1139/e81-019

Blichert-Toft, J., and Albarède, F., 1997, The Lu-Hf isotope geochemistry of chondrites and the evolution of the mantle-crust system: Earth and Planetary Science Letters, v. 148, n. 1–2, p. 243–258, https://doi.org/10.1016/S0012-821X(97)00040-X

Boulin, J., 1988, Hercynian and Eocimmerian events in Afghanistan and adjoining regions: Tectonophysics, v. 148, n. 3–4, p. 253–278, https://doi.org/10.1016/0040-1951(88)90134-5

Bouvier, A., Vervoort, J. D., and Patchett, P. J., 2008, The Lu–Hf and Sm–Nd isotopic composition of CHUR: constraints from unequilibrated chondrites and implications for the bulk composition of terrestrial planets: Earth and Planetary Science Letters, v. 273, n. 1–2, p. 48–57, https://doi.org/10.1016/j.epsl.2008.06.010

Brown, M., 2014, The contribution of metamorphic petrology to understanding lithosphere evolution and geodynamics: Geoscience Frontiers, v. 5, n. 4, p. 553–569, https://doi.org/10.1016/j.gsf.2014.02.005

Brunet, M. F., and Cloetingh, S., 2003, Integrated peri-Tethyan basins studies (peri-Tethys programme): Sedimentary Geology, v. 156, n. 1–4, p. 1–10, https://doi.org/10.1016/S0037-0738(02)00279-8

Brunet, M. F., Korotaev, M. V., Ershov, A. V., and Nikishin, A. M., 2003, The South Caspian Basin: a review of its evolution from subsidence modelling: Sedimentary Geology, v. 156, n. 1–4, p. 119–148, https://doi.org/10.1016/S0037-0738(02)00285-3

Cai, F., Ding, L., Wang, H., Laskowski, A. K., Zhang, L., Zhang, B., Mohammadi, A., Li, J., Song, P., Li, Z., and Zhang, Q., 2021, Configuration and timing of collision between Arabia and Eurasia in the Zagros collision zone, Fars, southern Iran: Tectonics, v. 40, n. 8, e2021TC006762 https://doi.org/10.1029/2021TC006762

Cawood, P. A., Hawkesworth, C. J., and Dhuime, B., 2012, Detrital zircon record and tectonic setting: Geology, v. 40, n. 10, p. 875–878, https://doi.org/10.1130/G32945.1

Cawood, P. A., Martin, E. L., Murphy, J. B., and Pisarevsky, S. A., 2021, Gondwana's interlinked peripheral orogens: Earth and Planetary Science Letters, v. 568, 117057 https://doi.org/10.1016/j.epsl.2021.117057

Chiu, H. Y., Chung, S. L., Zarrinkoub, M. H., Melkonyan, R., Pang, K. N., Lee, H. Y., Wang, K. L., Mohammadi, S. S., and Khatib, M. M., 2017, Zircon Hf isotopic constraints on magmatic and tectonic evolution in Iran: Implications for crustal growth in the Tethyan orogenic belt: Journal of Asian Earth Sciences, v. 145, Part B, p. 652–669, https://doi.org/10.1016/j.jseaes.2017.06.011

Chu, N. C., Taylor, R. N., Chavagnac, V., Nesbitt, R. W., Boella , R. M., Milton, J. A., German, C. R., Bayon, G., and Burton, K., 2002, Hf isotope ratio analysis using multi-collector inductively coupled plasma mass spectrometry: an evaluation of isobaric interference corrections: Journal of Analytical Atomic Spectrometry, v. 17, n. 12, p. 1567–1574, https://doi.org/10.1039/b206707b

Chu, Y., Wan, B., Allen, M. B., Chen, L., Lin, W., Talebian, M., and Xin, G., 2021, Detrital Zircon Age Constraints on the Evolution of Paleo-Tethys in NE Iran: Implications for Subduction and Collision Tectonics: Tectonics, v. 40, n. 8, e2020TC006680, https://doi.org/10.1029/2020TC006680

Debon, F., Afzali, H., Le Fort, P., and Sonet, J., 1987, Major intrusive stages in Afghanistan: typology, age and geodynamic setting: Geologische Rundschau, v. 76, n. 1, p. 245–264, https://doi.org/10.1007/BF01820586

Delavari, M., Dolati, A., Mohammadi, A., and Rostami, F., 2016, The Permian volcanics of central Alborz: implications for passive continental margin along the southern border of Paleotethys: Ofioliti, v. 41, n. 2, p. 59–74, https://doi.org/10.4454/ofioliti.v41i2.460

Derakhshi, M., and Ghasemi, H., 2015, Soltan Maidan Complex (SMC) in the eastern Alborz structural zone, northern Iran: magmatic evidence for Paleotethys development: Arabian Journal of Geosciences, v. 8, n. 2, p. 849–866, https://doi.org/10.1007/s12517-013-1180-2

Dickinson, W. R., 1985, Interpreting provenance relations from detrital modes of sandstones, Provenance of arenites, *in* Zuffa, G. G., editor, Provenance of Arenites: Dordrecht, Springer, NATO ASI Series, v. 148, p. 333–361, https://doi.org/10.1007/978-94-017-2809-6_15

Dickinson, W. R., and Suczek, C. A., 1979, Plate tectonics and sandstone compositions: AAPG Bulletin, v. 63, n. 12, p. 2164–2182, https://doi.org/10.1306/2F9188FB-16CE-11D7-8645000102C1865D

Dickson, J., 1966, Carbonate identification and genesis as revealed by staining: Journal of Sedimentary Research, v. 36, n. 2, p. 91–505, https://doi.org/10.1306/74D714F6-2B21-11D7-8648000102C1865D
Fedo, C. M., Sircombe, K. N., and Rainbird, R. H., 2003, Detrital zircon analysis of the sedimentary record: Reviews in Mineralogy and Geochemistry, v. 53, n. 1, p. 277–303, https://doi.org/10.2113/0530277
Gaetani, M., 1997, The Karakorum block in central Asia, from Ordovician to Cretaceous: Sedimentary Geology, v. 109, n. 3–4, p. 339–359, https://doi.org/10.1016/S0037-0738(96)00068-1
Garzanti, E., 2016, From static to dynamic provenance analysis—Sedimentary petrology upgraded: Sedimentary Geology, v. 336, p. 3–13, https://doi.org/10.1016/j.sedgeo.2015.07.010
Garzanti, E., 2017, The maturity myth in sedimentology and provenance analysis: Journal of Sedimentary Research, v. 87, n. 4, p. 353–365, https://doi.org/10.2110/jsr.2017.17
Garzanti, E., and Andò, S., 2019, Heavy minerals for junior woodchucks: Minerals, v. 9, n. 3, p. 148, https://doi.org/10.3390/min9030148
Gehrels, G., Kapp, P., DeCelles, P., Pullen, A., Blakey, R., Weislogel, A., Ding, L., Guynn, J., Martin, A., McQuarrie, N., and Yin, A., 2011, Detrital zircon geochronology of pre-Tertiary strata in the Tibetan-Himalayan orogen: Tectonics, v. 30, TC5016, https://doi.org/10.1029/2011TC002868
Ghaemi, F., 2009, Tectonic setting of sedimentary facies in the Kopet–Dagh Basement: Sedimentary Facies (in Persian), v. 2, n. 1, p. 61–79, https://doi.org/10.22067/SED.FACIES.V2I1.2071
Ghavi, J., Karimpour, M. H., Mazaheri, S. A., and Pan, Y., 2018, Triassic I-type granitoids from the Torbat e Jam area, northeastern Iran: Petrogenesis and implications for Paleotethys tectonics: Journal of Asian Earth Sciences, v. 164, p. 159–178, https://doi.org/10.1016/j.jseaes.2018.06.025
Ghavidel-Syooki, M., Hassanzadeh, J., and Vecoli, M., 2011, Palynology and isotope geochronology of the Upper Ordovician–Silurian successions (Ghelli and Soltan Maidan Formations) in the Khoshyeilagh area, eastern Alborz Range, northern Iran; stratigraphic and palaeogeographic implications: Review of Palaeobotany and Palynology, v. 164, n. 3–4, p. 251–271, https://doi.org/10.1016/j.revpalbo.2011.01.006
Ghazi, A. M., Hassanipak, A. A., Tucker, P. J., Mobasher, K., and Duncan, R. A., 2001, Geochemistry and 40Ar-39Ar ages of the Mashhad Ophiolite, NE Iran: A Rare Occurrence of a 300 Ma (Paleo-Tethys) Oceanic Crust: American Geophysical Union Fall Meeting Abstracts, p. V12C-0993.
Golonka, J., 2004, Plate tectonic evolution of the southern margin of Eurasia in the Mesozoic and Cenozoic: Tectonophysics, v. 381, n. 1–4, p. 235–273, https://doi.org/10.1016/j.tecto.2002.06.004
Gradstein, F. M., Ogg, G., and Schmitz, M., 2012, The Geologic Time Scale 2012: Amsterdam, the Netherlands, Elsevier, 1176 p.
Griffin, W. L., Pearson, N. J., Belousova, E., Jackson, S. E., van Achterbergh, E., O'Reilly, S. Y., and Shee, S. R., 2000, The Hf isotope composition of cratonic mantle: LAM-MC-ICPMS analysis of zircon megacrysts in kimberlites: Geochimica et Cosmochimica Acta, v. 64, n. 1, p. 133–147, https://doi.org/10.1016/S0016-7037(99)00343-9
Hanel, M., Gurbanov, A. G., and Lippolt, H. J., 1992, Age and genesis of granitoids from the Main-Range and Bechasyn zones of the western Great Caucasus: Neues Jahrbuch fur Mineralogie Monatshefte, v. 12, p. 529–544.
Hassanzadeh, J., Stockli, D. F., Horton, B. K., Axen, G. J., Stockli, L. D., Grove, M., Schmitt, A. K., and Walker, J. D., 2008, U-Pb zircon geochronology of late Neoproterozoic–Early Cambrian granitoids in Iran: Implications for paleogeography, magmatism, and exhumation history of Iranian basement: Tectonophysics, v. 451, n. 1–4, p. 71–96, https://doi.org/10.1016/j.tecto.2007.11.062
Hellstrom, J., Paton, C., Woodhead, J., and Hergt, J., 2008, Iolite: software for spatially resolved LA-(quad and MC) ICPMS analysis: Mineralogical Association of Canada short course series, v. 40, p. 343–348.
Hollingsworth, J., Jackson, J., Walker, R., Reza Gheitanchi, M., and Javad Bolourchi, M., 2006, Strike-slip faulting, rotation, and along-strike elongation in the Kopeh Dagh Mountains, NE Iran: Geophysical Journal International, v. 166, n. 3, p. 1161–1177, https://doi.org/10.1111/j.1365-246X.2006.02983.x
Hollingsworth, J., Fattahi, M., Walker, R., Talebian, M., Bahroudi, A., Bolourchi, M. J., Jackson, J., and Copley, A., 2010, Oroclinal bending, distributed thrust and strike-slip faulting, and the accommodation of Arabia–Eurasia convergence in NE Iran since the Oligocene: Geophysical Journal International, v. 181, n. 3, p. 1214–1246, https://doi.org/10.1111/j.1365-246X.2010.04591.x
Horstwood, M. S. A., Košler, J., Gehrels, G., Jackson, S. E., McLean, N. M., Paton, C., Pearson, N. J., Sircombe, K., Sylvester, P., Vermeesch, P., Bowring, J. F., Condon, D. J., and Schoene, B., 2016, Community-derived standards for LA-ICP-MS U-(Th-) Pb geochronology–Uncertainty propagation, age interpretation and data reporting: Geostandards and Geoanalytical Research, v. 40, n. 3, p. 311–332, https://doi.org/10.1111/j.1751-908X.2016.00379.x
Horton, B. K., Hassanzadeh, J., Stockli, D. F., Axen, G. J., Gillis, R. J., Guest, B., Amini, A., Fakhari, M. D., Zamanzadeh, S. M., and Grove, M., 2008, Detrital zircon provenance of Neoproterozoic to Cenozoic deposits in Iran: Implications for chronostratigraphy and collisional tectonics: Tectonophysics, v. 451, n. 1–4, p. 97–122, https://doi.org/10.1016/j.tecto.2007.11.063
Hosseini, S. H., Sadeghian, M., Zhai, M., and Ghasemi, H., 2015, Petrology, geochemistry and zircon U–Pb dating of Band-e-Hezarchah metabasites (NE Iran): An evidence for back-arc magmatism along the northern active margin of Gondwana: Geochemistry, v. 75, n. 2, p. 207–218, https://doi.org/10.1016/j.chemer.2015.02.002
Hubert, J. F., 1962, A zircon-tourmaline-rutile maturity index and the interdependence of the composition of heavy mineral assemblages with the gross composition and texture of sandstones: Journal of Sedimentary Research, v. 32, n. 3, p. 440–450, https://doi.org/10.1306/74D70CE5-2B21-11D7-8648000102C1865D
Ingersoll, R. V., Bullard, T. F., Ford, R. L., Grimm, J. P., Pickle, J. D., and Sares, S. W., 1984, The effect of grain size on detrital modes: a test of the Gazzi-Dickinson point-counting method: Journal of

Sedimentary Research, v. 54, n. 1, p. 103–116, https://doi.org/10.1306/212F83B9-2B24-11D7-8648000102C1865D
Karimpour, M. H., Stern, C. R., and Farmer, G. L., 2010, Zircon U–Pb geochronology, Sr–Nd isotope analyses, and petrogenetic study of the Dehnow diorite and Kuhsangi granodiorite (Paleo-Tethys), NE Iran: Journal of Asian Earth Sciences, v. 37, n. 4, p. 384–393, https://doi.org/10.1016/j.jseaes.2009.11.001
Kavoosi, M. A., Lasemi, Y., Sherkati, S., and Moussavi-Harami, R., 2009, Facies analysis and depositional sequences of the Upper Jurassic Mozduran Formation, a carbonate reservoir in the Kopet Dagh Basin, NE Iran: Journal of Petroleum Geology, v. 32, n. 3, p. 235–259, https://doi.org/10.1111/j.1747-5457.2009.00446.x
Lasemi, Y., 1995, Platform carbonates of the Upper Jurassic Mozduran formation in the Kopet Dagh Basin, NE Iran-facies, palaeoenvironments and sequences: Sedimentary Geology, v. 99, n. 3–4, p. 151–164, https://doi.org/10.1016/0037-0738(95)00041-6
Lechmann, A., Burg, J. P., Ulmer, P., Mohammadi, A., Guillong, M., and Faridi, M., 2018, From Jurassic rifting to Cretaceous subduction in NW Iranian Azerbaijan: geochronological and geochemical signals from granitoids: Contributions to Mineralogy and Petrology, v. 173, n. 12, 102 https://doi.org/10.1007/s00410-018-1532-8
Ludwig, K. R., 2003, User's manual for Isoplot 3.00: geochronological toolkit for Microsoft Excel: Berkeley, California, Berkeley Geochronology Center Special Publication, v. 4, 74 p.
Lyberis, N., and Manby , G., 1999, Oblique to orthogonal convergence across the Turan block in the post-Miocene: American Association of Petroleum Geologists Bulletin, v. 83, n. 7, p. 1135–1160, https://doi.org/10.1306/E4FD2E97-1732-11D7-8645000102C1865D
Mahboubi, A., Moussavi-Harami, R., Mansouri-Daneshvar, P., Nadjafi, M., and Brenner, R. L., 2006, Upper Maastrichtian depositional environments and sea-level history of the Kopet-Dagh Intracontinental Basin, Kalat Formation, NE Iran: Facies, v. 52, p. 237–248, https://doi.org/10.1007/s10347-005-0034-0
Mange, M. A., and Maurer, H. F., 1992, Heavy minerals in colour: London, United Kingdom, Chapman & Hall, 147 p., https://doi.org/10.1007/978-94-011-2308-2
Mangino, S., and Priestley, K., 1998, The crustal structure of the southern Caspian region: Geophysical Journal International, v. 133, n. 3, p. 630–648, https://doi.org/10.1046/j.1365-246X.1998.00520.x
Martens, J. H. C., 1932, Piperine as an immersion medium in sedimentary petrography: American Mineralogist, v. 17, n. 5, p. 198–199.
McQuarrie, N., Stock, J. M., Verdel, C., and Wernicke, B. P., 2003, Cenozoic evolution of Neotethys and implications for the causes of plate motions: Geophysical Research Letters, v. 30, n. 20, 2036, https://doi.org/10.1029/2003GL017992
Meinhold, G., Morton, A. C., and Avigad, D., 2013, New insights into peri-Gondwana paleogeography and the Gondwana super-fan system from detrital zircon U–Pb ages: Gondwana Research, v. 23, n. 2, p. 661–665, https://doi.org/10.1016/j.gr.2012.05.003
Meinhold, G., Bassis , A., Hinderer, M., Lewin, A., and Berndt, J., 2021, Detrital zircon provenance of north Gondwana Palaeozoic sandstones from Saudi Arabia: Geological Magazine, v. 158, n. 3, p. 442–458, https://doi.org/10.1017/S0016756820000576
Mirnejad, H., Lalonde, A. E., Obeid, M., and Hassanzadeh, J., 2013, Geochemistry and petrogenesis of Mashhad granitoids: An insight into the geodynamic history of the Paleo-Tethys in northeast of Iran: Lithos, v. 170–171, p. 105–116, https://doi.org/10.1016/j.lithos.2013.03.003
Moghadam, H. S., Li, X. H., Ling, X. X., Stern, R. J., Khedr, M. Z., Chiaradia, M., Ghorbani, G., Arai , S., and Tamura, A., 2015a, Devonian to Permian evolution of the Paleo-Tethys Ocean: new evidence from U–Pb zircon dating and Sr–Nd–Pb isotopes of the Darrehanjir–Mashhad "ophiolites", NE Iran: Gondwana Research, v. 28, n. 2, p. 781–799, https://doi.org/10.1016/j.gr.2014.06.009
Moghadam, H. S., Khademi, M., Hu, Z., Stern, R. J., Santos, J. F., and Wu, Y., 2015b, Cadomian (Ediacaran–Cambrian) arc magmatism in the ChahJam–Biarjmand metamorphic complex (Iran): Magmatism along the northern active margin of Gondwana: Gondwana Research, v. 27, n. 1, p. 439–452, https://doi.org/10.1016/j.gr.2013.10.014
Moghadam, H. S., Li, X. H., Santos, J. F., Stern, R. J., Griffin, W. L., Ghorbani, G., and Sarebani, N., 2017, Neoproterozoic magmatic flare-up along the N. margin of Gondwana: The Taknar complex, NE Iran: Earth and Planetary Science Letters, v. 474, p. 83–96, https://doi.org/10.1016/j.epsl.2017.06.028
Moghadam, H. S., Li, Q. L., Griffin, W. L., Stern, R. J., Ishizuka, O., Henry, H., Lucci, F., O'Reilly, S. Y., and Ghorbani, G., 2020, Repeated magmatic buildup and deep "hot zones" in continental evolution: The Cadomian crust of Iran: Earth and Planetary Science Letters, v. 531, 115989, https://doi.org/10.1016/j.epsl.2019.115989
Mohammadi, A., Burg, J. P., and Winkler, W., 2016a, Detrital zircon and provenance analysis of Eocene–Oligocene strata in the South Sistan suture zone, southeast Iran: Implications for the tectonic setting: Lithosphere, v. 8, n. 6, p. 615–632, https://doi.org/10.1130/L538.1
Mohammadi, A., Burg, J. P., Winkler, W., Ruh, J., and von Quadt, A., 2016b, Detrital zircon and provenance analysis of Late Cretaceous-Miocene onshore Iranian Makran strata: Implications for the tectonic setting: Geological Society of America Bulletin, v. 128, n. 9–10, p. 1481–1499, https://doi.org/10.1130/B31361.1
Mohammadi, A., Burg, J. P., Guillong, M., and von Quadt, A., 2017, Arc magmatism witnessed by detrital zircon U-Pb geochronology, Hf isotopes and provenance analysis of Late Cretaceous-Miocene sandstones of onshore western Makran (SE Iran): American Journal of Science, v. 317, n. 8, p. 941–964, https://doi.org/10.2475/08.2017.03
Mohammadi, A., Moazzen, M., Lechmann, A., and Laurent, O., 2020, Zircon U-Pb geochronology and geochemistry of Late Devonian–Carboniferous granitoids in NW Iran: implications for the opening of Paleo-Tethys: International Geology Review, v. 62, n. 15, p. 1931–1948, https://doi.org/10.1080/00206814.2019.1675540

Mohammadi, A., Burg, J. P., and Guillong, M., 2022, The Siah Cheshmeh-Khoy-Misho-Tabriz fault (NW Iran) is a cryptic neotethys suture: evidence from detrital zircon geochronology, Hf isotopes, and provenance analysis: International Geology Review, v. 64, n. 2, p. 182–202, https://doi.org/10.1080/00206814.2020.1845992

Morag, N., Avigad, D., Gerdes, A., and Harlavan, Y., 2012, 1000–580 Ma crustal evolution in the northern Arabian-Nubian Shield revealed by U–Pb–Hf of detrital zircons from late Neoproterozoic sediments (Elat area, Israel): Precambrian Research, v. 208–211, p. 197–212, https://doi.org/10.1016/j.precamres.2012.04.009

Morel, M. L. A., Nebel, O., Nebel-Jacobsen, Y. J., Miller, J. S., and Vroon , P. Z., 2008, Hafnium isotope characterization of the GJ-1 zircon reference material by solution and laser-ablation MC-ICPMS: Chemical Geology, v. 255, n. 1–2, p. 231–235, https://doi.org/10.1016/j.chemgeo.2008.06.040

Mortazavi, M., and Moussavi-Harami, R., and Mahboubi, A., 2013, Detrital mode and geochemistry of the Shurijeh Formation (Late Jurassic-Early Cretaceous) in the central and western parts of the intracontinental Kopet-Dagh Basin, NE Iran: Implications for provenance, tectonic setting and weathering processes: Acta Geologica Sinica-English Edition, v. 87, n. 4, p. 1058–1080, https://doi.org/10.1111/1755-6724.12110

Mortazavi , M., Moussavi-Harami , R., Mahboubi , A., and Nadjafi , M., 2014, Geochemistry of the Late Jurassic–Early Cretaceous shales (Shurijeh Formation) in the intracontinental Kopet-Dagh Basin, northeastern Iran: implication for provenance, source weathering, and paleoenvironments: Arabian Journal of Geosciences, v. 7, n. 12, p. 5353–5366, https://doi.org/10.1007/s12517-013-1081-4

Moussavi-Harami, R., 1993, Depositional history and paleogeography of the lower Paleocene redbeds in eastern Kopet-Dagh Basin Northeastern Iran: Journal of Science Islamic Republic of Iran, v. 4, n. 2, p. 126–143.

Moussavi-Harami, R., and Brenner, R. L., 1990, Lower Cretaceous (Neocomian) fluvial deposits in eastern Kopet-Dagh basin, northeastern Iran: Cretaceous Research, v. 11, n. 2, p. 163–174, https://doi.org/10.1016/S0195-6671(05)80031-X

Moussavi-Harami, R., and Brenner, R. L., 1993, Diagenesis of non-marine petroleum reservoirs: The Neocomian (Lower Cretaceous) Shurijeh Formation, Kopet-Dagh Basin, NE Iran: Journal of Petroleum Geology, v. 16, n. 1, p. 55–72, https://doi.org/10.1111/j.1747-5457.1993.tb00730.x

Muttoni, G., Mattei, M., Balini, M., Zanchi, A., Gaetani, M., and Berra, F., 2009, The drift history of Iran from the Ordovician to the Triassic: Geological Society, London, Special Publications, v. 312, n. 1, p. 7–29, https://doi.org/10.1144/SP312.2

Natalin, B. A., and Şengör, A. C., 2005, Late Palaeozoic to Triassic evolution of the Turan and Scythian platforms: the pre-history of the Palaeo-Tethyan closure: Tectonophysics, v. 404, n. 3–4, p. 175–202, https://doi.org/10.1016/j.tecto.2005.04.011

Norman, M. B., 1974, Improved techniques for selective staining of feldspar and other minerals using amaranth: Journal of Research of the US Geological Survey, v. 2, n. 1, p. 73–79.

Nowrouzi, Z., Moussavi-Harami, R., Mahboubi, A., Gharaie, M. H. M., and Ghaemi, F., 2014, Petrography and geochemistry of Silurian Niur sandstones, Derenjal Mountains, East Central Iran: implications for tectonic setting, provenance and weathering: Arabian Journal of Geosciences, v. 7, n. 7, p. 2793–2813, https://doi.org/10.1007/s12517-013-0912-7

Okay, A. I., Sunal, G., Sherlock, S., Altıner, D., Tüysüz, O., and Kylander-Clark, A.R. C., and Aygül, M., 2013, Early Cretaceous sedimentation and orogeny on the active margin of Eurasia: Southern Central Pontides, Turkey: Tectonics, v. 32, n. 5, p. 1247–1271, https://doi.org/10.1002/tect.20077

Patchett, P. J., 1983, Hafnium isotope results from mid-ocean ridges and Kerguelen: Lithos, v. 16, n. 1, p. 47–51, https://doi.org/10.1016/0024-4937(83)90033-6

Paton, C., Woodhead, J. D., Hellstrom, J. C., Hergt, J. M., Greig, A., and Maas, R., 2010, Improved laser ablation U-Pb zircon geochronology through robust downhole fractionation correction: Geochemistry, Geophysics, Geosystems, v. 11, n. 3, Q0AA06 https://doi.org/10.1029/2009GC002618

Petrus, J. A., and Kamber, B. S., 2012, Vizual Age: A novel approach to laser ablation ICP-MS U-Pb geochronology data reduction: Geostandards and Geoanalytical Research, v. 36, n. 3, p. 247–270, https://doi.org/10.1111/j.1751-908X.2012.00158.x

Poursoltani, M. R., and Gibling, M. R., 2011, Composition, porosity, and reservoir potential of the Middle Jurassic Kashafrud Formation, northeast Iran: Marine and Petroleum Geology, v. 28, n. 5, p. 1094–1110, https://doi.org/10.1016/j.marpetgeo.2010.11.004

Poursoltani, M. R., Moussavi-Harami, R., and Gibling, M. R., 2007, Jurassic deep-water fans in the Neo-Tethys Ocean: the Kashafrud Formation of the Kopet-Dagh basin, Iran: Sedimentary Geology, v. 198, n. 1–2, p. 53–74, https://doi.org/10.1016/j.sedgeo.2006.11.004

Ramezani, J., and Tucker, R. D., 2003, The Saghand region, central Iran: U-Pb geochronology, petrogenesis and implications for Gondwana tectonics: American Journal of Science, v. 303, n. 7, p. 622–665, https://doi.org/10.2475/ajs.303.7.622

Robert, A. M. M., Letouzey, J., Kavoosi, M. A., Sherkati, S., Müller, C., Vergés, J., and Aghababaei, A., 2014, Structural evolution of the Kopeh Dagh fold-and-thrust belt (NE Iran) and interactions with the South Caspian Sea Basin and Amu Darya Basin: Marine and Petroleum Geology, v. 57, p. 68–87, https://doi.org/10.1016/j.marpetgeo.2014.05.002

Ruh, J. B., and Vergés, J., 2018, Effects of reactivated extensional basement faults on structural evolution of fold-and-thrust belts: Insights from numerical modelling applied to the Kopet Dagh Mountains: Tectonophysics, v. 746, p. 493–511, https://doi.org/10.1016/j.tecto.2017.05.020

Scherer, E., Münker, C., and Mezger, K., 2001, Calibration of the lutetium-hafnium clock: Science, v. 293, n. 5530, p. 683–687, https://doi.org/10.1126/science.1061372

Şengör, A. M. C., 1990a, Plate tectonics and orogenic research after 25 years: A Tethyan perspective: Earth Science Reviews, v. 27, n. 1–2, p. 1–201, https://doi.org/10.1016/0012-8252(90)90002-D

Şengör, A. M. C., 1990b, A new model for the late Palaeozoic-Mesozoic tectonic evolution of Iran and implications for Oman: Geological Society, London, Special Publications, v. 49, n. 1, p. 797–831, https://doi.org/10.1144/GSL.SP.1992.049.01.49

Şengör, A. M. C., Yılmaz, Y., and Sungurlu, O., 1984, Tectonics of the Mediterranean Cimmerides: nature and evolution of the western termination of Palaeo-Tethys: Geological Society, London, Special Publications, v. 17, n. 1, p. 77–112, https://doi.org/10.1144/GSL.SP.1984.017.01.04

Sláma, J., Košler, J., Condon, D. J., Crowley, J. L., Gerdes, A., Hanchar, J. M., Horstwood, M. S. A., Morris, G. A., Nasdala, L., Norberg, N., Schaltegger, U., Schoene, B., Tubrett, M. N., and Whitehouse, M. J., 2008, Plešovice zircon—a new natural reference material for U–Pb and Hf isotopic microanalysis: Chemical Geology, v. 249, n. 1–2, p. 1–35, https://doi.org/10.1016/j.chemgeo.2007.11.005

Stampfli, G. M., 2000, Tethyan oceans: Geological society, London, special publications, v. 173, n. 1, p. 1–23, https://doi.org/10.1144/GSL.SP.2000.173.01.01

Stampfli, G. M., and Borel, G. D., 2002, A plate tectonic model for the Paleozoic and Mesozoic constrained by dynamic plate boundaries and restored synthetic oceanic isochrons: Earth and Planetary Science Letters, v. 196, n. 1–2, p. 17–33, https://doi.org/10.1016/S0012-821X(01)00588-X

Stampfli, G. M., Hochard, C., Vérard, C., Wilhem , C., and vonRaumer, J., 2013, The formation of Pangea: Tectonophysics, v. 593, p. 1–19, https://doi.org/10.1016/j.tecto.2013.02.037

Stöcklin, J., 1974, Possible ancient continental margins in Iran, *in* Burk, C. A., and Drake, C. L., editors, The geology of continental margins: Springer, Berlin, Heidelberg, p. 873–887, https://doi.org/10.1007/978-3-662-01141-6_64

Thomas, J. C., Grasso, J. R., Bossu, R., Martinod, J., and Nurtaev, B., 1999, Recent deformation in the Turan and South Kazakh platforms, western central Asia, and its relation to Arabia-Asia and India-Asia collisions: Tectonics, v. 18, n. 2, p. 201–214, https://doi.org/10.1029/1998TC900027

Topuz, G., Hegner, E., Homam, S. M., Ackerman, L., Pfänder, J. A., and Karimi, H., 2018, Geochemical and geochronological evidence for a Middle Permian oceanic plateau fragment in the Paleo-Tethyan suture zone of NE Iran: Contributions to Mineralogy and Petrology, v. 173, n. 10, p. 1–23, https://doi.org/10.1007/s00410-018-1506-x

Topuz, G., Candan, O., Okay, A. I., von Quadt, A., Othman, M., Zack, T., and Wang, J., 2020, Silurian anorogenic basic and acidic magmatism in Northwest Turkey: Implications for the opening of the Paleo-Tethys: Lithos, v. 356–357, 105302 https://doi.org/10.1016/j.lithos.2019.105302

Topuz, G., Candan, O., Wang, J. M., Li, Q. L., Wu, F. Y., and Yılmaz, A., 2021, Silurian A-type metaquartzsyenite to-granite in the Eastern Anatolia: Implications for Late Ordovician-Silurian rifting at the northern margin of Gondwana: Gondwana Research, v. 91, p. 1–17, https://doi.org/10.1016/j.gr.2020.12.005

Vaezi Pour, M. J., Behrouzi, A., Alavi Tehrani, N., Kholghi, M. H., and Alavi Naini, M., 1992, Torbat-e-Heydarieh geological quadrangle map: Geological survey of Iran, scale 1:250,000.

Vermeesch, P., Rittner, M., Petrou, E., Omma, J., Mattinson, C., and Garzanti, E., 2017, High throughput petrochronology and sedimentary provenance analysis by automated phase mapping and LAICPMS: Geochemistry, Geophysics, Geosystems, v. 18, n. 11, p. 4096–4109, https://doi.org/10.1002/2017GC007109

Weislogel, A. L., Graham, S. A., Chang, E. Z., Wooden, J. L., Gehrels, G. E., and Yang, H., 2006, Detrital zircon provenance of the Late Triassic Songpan-Ganzi complex: Sedimentary record of collision of the North and South China blocks: Geology, v. 34, n. 2, p. 97–100, https://doi.org/10.1130/G21929.1

Weltje, G. J., and von Eynatten, H., 2004, Quantitative provenance analysis of sediments: review and outlook: Sedimentary Geology, v. 171, n. 1–4, p. 1–11, https://doi.org/10.1016/j.sedgeo.2004.05.007

Wiedenbeck, M., Allé, P., Corfu, F., Griffin, W. L., Meier, M., Oberli, F., Von Quadt, A., Roddick, J. C., and Spiegel, W., 1995, Three natural zircon standards for U-Th-Pb, Lu-Hf, trace element and REE analyses: Geostandards Newsletter, v. 19, n. 1, p. 1–23, https://doi.org/10.1111/j.1751-908X.1995.tb00147.x

Wilmsen, M., Fürsich, F. T., and Seyed-Emami, K., Majidifard, M. R., and Taheri, J., 2009, The Cimmerian Orogeny in northern Iran: Tectono-stratigraphic evidence from the foreland: Terra Nova, v. 21, n. 3, p. 211–218, https://doi.org/10.1111/j.1365-3121.2009.00876.x

Woodhead, J. D., and Hergt, J. M., 2005, A preliminary appraisal of seven natural zircon reference materials for in situ Hf isotope determination: Geostandards and Geoanalytical Research, v. 29, n. 2, p. 183–195, https://doi.org/10.1111/j.1751-908X.2005.tb00891.x

Woodhead, J., Hergt, J., Shelley, M., Eggins, S., and Kemp, R., 2004, Zircon Hf-isotope analysis with an excimer laser, depth profiling, ablation of complex geometries, and concomitant age estimation: Chemical Geology, v. 209, n. 1–2, p. 121–135, https://doi.org/10.1016/j.chemgeo.2004.04.026

Zanchetta, S., Berra, F., Zanchi, A., Bergomi, M., Caridroit, M., Nicora, A., and Heidarzadeh, G., 2013, The record of the Late Palaeozoic active margin of the Palaeotethys in NE Iran: constraints on the Cimmerian orogeny: Gondwana Research, v. 24, n. 3–4, p. 1237–1266, https://doi.org/10.1016/j.gr.2013.02.013

Zanchi, A., Berra, F., Mattei, M., Ghassemi, M. R., and Sabouri, J., 2006, Inversion tectonics in central Alborz, Iran: Journal of Structural Geology, v. 28, n. 11, p. 2023–2037, https://doi.org/10.1016/j.jsg.2006.06.020

Zanchi, A., Zanchetta, S., Berra, F., Mattei, M., Garzanti, E., Molyneux, S., Nawab, A., and Sabouri, J., 2009, The Eo-Cimmerian (Late? Triassic) orogeny in North Iran: Geological Society, London, Special Publications, v. 312, n. 1, p. 31–55, https://doi.org/10.1144/SP312.3

Zanchi, A., Zanchetta, S., Balini, M., and Ghassemi, M. R., 2016, Oblique convergence during the Cimmerian collision: evidence from the Triassic Aghdarband Basin, NE Iran: Gondwana Research, v. 38, p. 149–170, https://doi.org/10.1016/j.gr.2015.11.008

Zoleikhaei, Y., Mulder, J. A., and Cawood, P. A., 2021, Integrated detrital rutile and zircon provenance reveals multiple sources for Cambrian sandstones in North Gondwana: Earth-Science Reviews, v. 213, 103462 https://doi.org/10.1016/j.earscirev.2020.103462

Zuffa, G. G., 1985, Optical analyses of arenites: Influence of methodology on compositional results, *in* Zuffa, G. G., editor, Provenance of arenites: Dordrecht, Springer, NATO ASI Series, v. 148, p. 165–189, https://doi.org/10.1007/978-94-017-2809-6_8